AD_____

GRANT NUMBER DAMD17-94-J-4126

TITLE: Development of Efficient Dynamic Magnetic Resonance Imaging Methods with Application to Breast Cancer Detection and Diagnosis

PRINCIPAL INVESTIGATOR: Dr. Paul Lauterbur
Jill M. Hanson

CONTRACTING ORGANIZATION: University of Illinois
Urbana, Illinois 61801

REPORT DATE: September 1996

TYPE OF REPORT: Annual

PREPARED FOR: Commander
U.S. Army Medical Research and Materiel Command
Fort Detrick, Frederick, Maryland 21702-5012

DISCLAIMER NOTICE

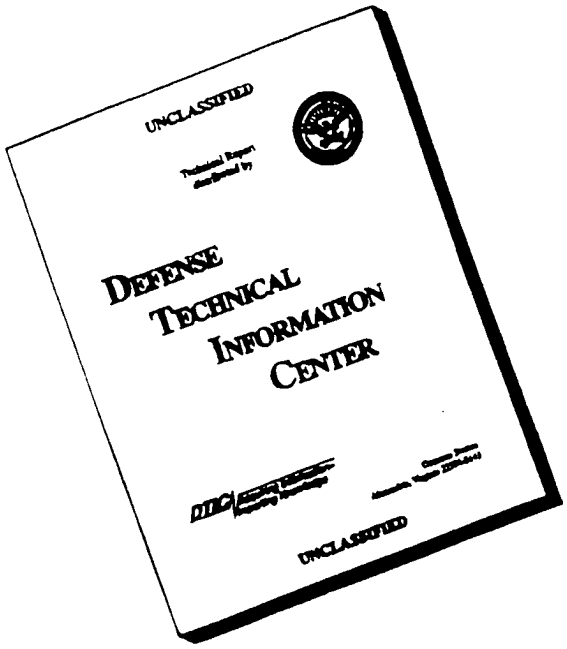

THIS DOCUMENT IS BEST QUALITY AVAILABLE. THE COPY FURNISHED TO DTIC CONTAINED A SIGNIFICANT NUMBER OF PAGES WHICH DO NOT REPRODUCE LEGIBLY.

REPORT DOCUMENTATION PAGE

Form Approved
OMB No. 0704-0188

1. AGENCY USE ONLY *(Leave blank)*	2. REPORT DATE	3. REPORT TYPE AND DATES COVERED
	September 1996	Annual (1 Sep 95 - 31 Aug 96)

4. TITLE AND SUBTITLE Development of Efficient Dynamic Magnetic Resonance Imaging Methods with Application to Breast Cancer Detection and Diagnosis

5. FUNDING NUMBERS

DAMD17-94-J-4126

6. AUTHOR(S)

Dr. Paul Lauterbur
Jill M. Hanson

7. PERFORMING ORGANIZATION NAME(S) AND ADDRESS(ES)

University of Illinois
Urbana, Illinois 61801

8. PERFORMING ORGANIZATION REPORT NUMBER

9. SPONSORING/MONITORING AGENCY NAME(S) AND ADDRESS(ES)

Commander
U.S. Army Medical Research and Materiel Command
Fort Detrick, MD 21702-5012

10. SPONSORING/MONITORING AGENCY REPORT NUMBER

11. SUPPLEMENTARY NOTES

12a. DISTRIBUTION / AVAILABILITY STATEMENT

Approved for public release; distribution unlimited

12b. DISTRIBUTION CODE

13. ABSTRACT *(Maximum 200*

The goal of this predoctoral fellowship research project is to improve the temporal and spatial resolutions in dynamic contrast-enhanced magnetic resonance imaging of the breast by optimizing the Reduced-encoding Imaging by Generalized-series Reconstruction (RIGR) method. Specifically, we investigated the use of non-Fourier encoding for collecting the reduced encoding dynamic data sets. The conclusion from our study was that the current SVD encoding method biases the results towards reproducing the known features in the reference image and, therefore, is not appropriate for dynamic imaging applications. For that reason, we continue to acquire the dynamic data using Fourier encoding. Next, we incorporated dynamic information into the basis functions of the generalized-series model used by the RIGR algorithm. The TRIGR method resulted from incorporating information about the dynamic changes into the basis functions. Explicit edge constraints derived from the reference image were then used along with the contrast information from the dynamic data to inject dynamic information into the basis functions for both RIGR and TRIGR. Of these, the TRIGR method works better for contrast-enhanced imaging because the active reference image can be used for the edge extraction step.

14. SUBJECT TERMS	15. NUMBER OF PAGES
Magnetic Resonance, Dynamic Imaging, Image Reconstruction, Constrained Image Reconstruction, Generalized Series, Inverse Problems, Breast Cancer	51
	16. PRICE CODE

17. SECURITY CLASSIFICATION OF REPORT	18. SECURITY CLASSIFICATION OF THIS PAGE	19. SECURITY CLASSIFICATION OF ABSTRACT	20. LIMITATION OF ABSTRACT
Unclassified	Unclassified	Unclassified	Unlimited

FOREWORD

Opinions, interpretations, conclusions and recommendations are those of the author and are not necessarily endorsed by the US Army.

____ Where copyrighted material is quoted, permission has been obtained to use such material.

____ Where material from documents designated for limited distribution is quoted, permission has been obtained to use the material.

____ Citations of commercial organizations and trade names in this report do not constitute an official Department of Army endorsement or approval of the products or services of these organizations.

____ In conducting research using animals, the investigator(s) adhered to the "Guide for the Care and Use of Laboratory Animals," prepared by the Committee on Care and Use of Laboratory Animals of the Institute of Laboratory Resources, National Research Council (NIH Publication No. 86-23, Revised 1985).

____ For the protection of human subjects, the investigator(s) adhered to policies of applicable Federal Law 45 CFR 46.

____ In conducting research utilizing recombinant DNA technology, the investigator(s) adhered to current guidelines promulgated by the National Institutes of Health.

____ In the conduct of research utilizing recombinant DNA, the investigator(s) adhered to the NIH Guidelines for Research Involving Recombinant DNA Molecules.

____ In the conduct of research involving hazardous organisms, the investigator(s) adhered to the CDC-NIH Guide for Biosafety in Microbiological and Biomedical Laboratories.

Jill M Hanson 9/24/96

PI - Signature Date

Contents

4 Introduction

The goal of this fellowship research project is to improve the temporal and spatial resolutions in dynamic contrast-enhanced magnetic resonance imaging (MRI) of the breast. The motivation for this is that dynamic contrast-enhanced MRI may be able to determine non-invasively whether a lesion is benign or malignant based on both the temporal enhancement curve in the lesion as well as the spatial pattern of enhancement in the tumor (1–11). To capitalize on the time of greatest differentiation between malignant and benign lesions, a sequence of images of the breast must be acquired during the first 1 or 2 minutes following contrast injection (12, 13). This leads to a requirement for simultaneously high spatial and temporal resolutions.

However, this is difficult with conventional MRI techniques since the requirements for increasing the temporal and spatial resolutions are conflicting. Traditionally, dynamic imaging was performed by acquiring a full high-resolution data set for each dynamic image. The data acquisition time for such a data set is dependent upon the excitation sequence. If the popular Fourier encoding sequence is used, then N_x excitations are necessary to acquire the data set if y is the frequency encoding direction and x is the phase encoding direction. Then, the total imaging time will be

$$T = N_x T_R \tag{1}$$

where T_R is the repetition time. Clearly, a straightforward way to shorten the imaging time is to reduce N_x. However, with the standard Fourier reconstruction method, the spatial resolution of the resulting image is

$$\Delta x = \frac{1}{N_x \Delta k_x}. \tag{2}$$

Therefore, an improvement in temporal resolution by reducing N_x is accompanied by a commensurate loss in spatial resolution.

To overcome this problem, several reduced scan methods have been proposed which use *a priori* information to reduce the number of dynamic encodings needed per dynamic image. These methods are characterized by the data acquisition scheme illustrated in Fig. 1 in which a single high-resolution reference data set is acquired, followed by a series of reduced dynamic encodings. These methods can be roughly grouped into two categories: non-Fourier encoding methods and constrained reconstruction methods.

The non-Fourier encoding methods, such as the wavelet (14–38) and singular value decomposition (SVD) (39–46) methods, use the *a priori* information during the data acquisition step to try to perform an optimal encoding of the dynamic image. By using these non-Fourier basis functions, they hope that the image can be well represented with fewer encodings, leading to improved temporal resolution.

On the other hand, the constrained reconstruction techniques use the *a priori* information during the data acquisition step. Examples of constrained reconstruction techniques are the Reduced-encoding Imaging by Generalized-series Reconstruction (RIGR) (47, 48) and Keyhole (49, 50) methods. The main difference between the methods is in the reconstruction of the dynamic images. In Keyhole, reference data is directly substituted for the unmeasured dynamic data prior to Fourier inversion. Although the method has been applied to dynamic breast imaging (51, 52) due to its simplicity, it can only track dynamic changes at low resolution (53, 54). In addition, image artifacts can arise due to data inconsistency between the reference and dynamic data sets, especially in contrast-enhanced imaging since the inflow of the contrast agent causes an increase in the overall intensity level as well as the intensity in the enhancing areas. These problems can cause improper diagnosis due to missed lesions (55).

The RIGR method tries to generate the missing dynamic data by using a generalized-series model (47, 48)

$$\hat{I}_{\text{dyn}}(x) = |I_{\text{ref}}(x)| \sum_{n=-N/2}^{N/2-1} c_n \, e^{i2\pi n \Delta k x} \tag{3}$$

where I_{ref} is the high-resolution reference image, N is the number of dynamic encodings, and Δk is the phase encoding step in k-space. The N model parameters c_n are determined by the constraint that the generated data should be identical to the actual measured data d_{dyn} at all sampled k-space points, which leads to

$$d_{\text{dyn}}(m) = \sum_{n=-N/2}^{N/2-1} c_n \, \hat{d}_{\text{ref}}(m-n) \qquad -N/2 \le m \le N/2-1 \tag{4}$$

where

$$\hat{d}_{\text{ref}}(m-n) = \int_{-\infty}^{\infty} |I_{\text{ref}}(x)| e^{-i2\pi(m-n)\Delta k x} dx. \tag{5}$$

Substituting the resulting coefficients into Eq. [3] will yield the desired dynamic image. RIGR can reconstruct the dynamic images with a higher spatial resolution than is pos-

sible with Keyhole because the basis functions of the generalized series model contain high-resolution information from the reference image. This has important ramifications for dynamic imaging.

The purpose of this fellowship research project is to improve the temporal and spatial resolution in contrast-enhanced dynamic imaging of the breast. Specifically, we seek to use the edge information from the reference data set and the contrast information in the dynamic data set to build the generalized-series basis functions for the RIGR method. By having dynamic information in the basis functions, as well as in the generalized-series coefficients, improved dynamic images should be obtained.

5 Completed Research

5.1 Fourier versus Non-Fourier Encoding

Given that a high-resolution reference image and N dynamic Fourier encodings are available, RIGR is an optimal way to mix the reference and dynamic data sets. However, the flexibility of MRI permits a wide variety of encoding schemes, leading one to wonder if there is a better way of acquiring the data than with the infinite exponentials used by the Fourier encoding method. This is the motivation behind the non-Fourier encoding reduced scan methods which include the wavelet and singular value decomposition (SVD) encoding methods. Based on signal processing theory, the truncated SVD is the optimal representation of the image for a given number of basis functions (encodings) in the least mean squared error sense. For this reason, we investigated the SVD encoding concept.

The SVD encoding method proposed by Cao, et al (39,40) and Zientara, et al (41–46) can be characterized by the following steps:

1. Acquire a high-resolution reference image using conventional Fourier encoding.

2. Perform the singular value decomposition (SVD) of this reference image as

$$I_{\text{ref}} = U \Sigma V^H \tag{6}$$

where U, Σ and V are the matrices containing the left singular vectors u_i, singular values σ_i and right singular vectors v_i, respectively.

3. Acquire the dynamic data using spatially selective RF pulses. For SVD encoding along the vertical or horizontal directions, the u_i or v_i, respectively, corresponding to the largest N singular values are selected for encoding the dynamic images. For the pure vertical encoding case, this can be expressed as

$$S_{\text{dyn}} = U_N^H \, I_{\text{dyn}} \tag{7}$$

where U_N is the matrix constructed from the N selected left singular vectors.

4. Reconstruct the dynamic images using SVD synthesis. This can be expressed mathematically as multiplying the dynamic data by U_N as

$$\hat{I}_{\text{dyn}} = U_N \, S_{\text{dyn}}. \tag{8}$$

A modification of the basic SVD method known as the SVD-Keyhole method (45) has a few additional steps. Specifically, these steps are

5. Create the eigenimage

$$I_{\text{ref},M-N} = U_{M-N} \, \Sigma_{M-N} \, V_{M-N}^H \tag{9}$$

where U_{M-N}, Σ_{M-N} and V_{M-N} are truncated matrices consisting of the $M - N$ least significant left singular vectors, singular values and right singular vectors, respectively.

6. Create the SVD-Keyhole image by adding $I_{\text{ref},M-N}$ to $\hat{I}_{\text{dyn}}$ given in Eq. [8] such that

$$\hat{\hat{I}}_{\text{dyn}} = U_N \, S_{\text{dyn}} + I_{\text{ref},M-N}. \tag{10}$$

To simulate the RIGR data acquisition, k-space data sets were generated from a sequence of high-resolution images. A baseline high-resolution data set was used as the reference data, and the central N phase encodings from the remaining data sets were used as the dynamic phase encodings. To simulate the SVD and SVD-Keyhole imaging methods, the singular value decomposition of the reference image was calculated according to Eq. [6]. The dynamic data were then generated using Eq. [7].

Based on our investigation into non-Fourier encoding (56, 57), we concluded that the current SVD data acquisition scheme biased the results towards reproducing the

known features in the reference image. An example of this is shown in Fig. 3 which uses the contrast-enhanced breast simulation model which was developed for this project last year. The dynamic changes include a variable rate of enhancement in each of the "lesions" as well as a slow overall background tissue enhancement. Images (a) and (b) show the reference and dynamic images, respectively, reconstructed using 128 phase encodings with the standard Fourier reconstruction method. Images (c)-(e) show the dynamic image reconstructed using 16 dynamic encodings with the SVD, SVD-Keyhole and RIGR, respectively. In addition to having fewer artifacts, the RIGR reconstruction faithfully reproduces the signal magnitudes in the lesions whereas the SVD methods do not. This is quantified in Fig. 4 which shows the average signal magnitudes in each of the four lesions as reproduced by the different methods. The SVD methods assign nearly the same signal magnitude to each of the lesions whereas the RIGR values are very close to the actual values as determined by the high-resolution dynamic image (b).

The methods were also tested on real MRI data provided by Dr. Erik Wiener from a contrast-enhanced dynamic imaging study of a rat with a large breast tumor. A high-resolution pre-contrast reference data set was obtained using a spin echo sequence (TR300/TE20). A series of full data sets was acquired as the contrast agent was injected and as it washed into the tumor. The dynamic data for the RIGR and SVD methods were generated as discussed earlier. Figure 5 (a) and (b) are the reference and dynamic images, respectively, reconstructed using 256 phase encodings with the standard Fourier reconstruction method. Images (c)-(e) show the dynamic image reconstructed with 32 dynamic encodings using SVD, SVD-Keyhole and RIGR, respectively. The RIGR image shows improved reconstruction of the internal details of the tumor, such as those indicated by the arrows.

The SVD methods also had difficulty detecting new features which arose due to dynamic changes. This is illustrated in Fig. 6 which shows a needle biopsy simulation. Images (a) and (b) are the reference and dynamic images, respectively, reconstructed using 256 phase encodings. Images (c)-(e) show the dynamic image reconstructed using 32 dynamic encodings with SVD, SVD-Keyhole and RIGR, respectively. In the RIGR image, since the reference image contains no information about the needle, Gibbs ringing results from this new feature. However, this artifact is much less serious than those arising from the SVD methods, which result in a wide needle reconstruction which

appears displaced from the proper location (indicated by the arrow). This artifact is not due to the truncation of the SVD representation but is due to the particular encoding vectors selected. To show this, Fig. 7 was reconstructed with the optimal 32 dynamic encodings as determined from the dynamic image itself. The greatly improved reconstruction of the needle attests the non-optimality of the reference encoding for representing the dynamic image.

From a signal processing perspective, the truncated SVD representation yields the reconstructed image with the least mean squared error for a given number of encodings. By using these singular vectors for encoding, the aim is to do an optimal encoding of the dynamic image. If optimal encoding could be achieved, neither RIGR nor any other technique could beat it. However, we have shown that the current SVD encoding method does not in general produce better images than RIGR. The reason for this is that the SVD encodings are optimal only with respect to the reference image and are sub-optimal with respect to the dynamic image (39). In fact, because singular vectors can be very sensitive to perturbation of a matrix (image) (58), the singular vectors derived from the reference image are not just sub-optimal, but they bias the acquisition towards reproducing the dominant features of the reference image. As a result, the SVD methods have a reduced capability to capture new dynamic features and contrast changes in existing image features. For this reason, SVD encoding is not appropriate for dynamic imaging applications.

This research generated a conference talk at the 4th Annual Meeting of the Society of Magnetic Resonance (see Appendix A), and a manuscript has been submitted for publication in *Magnetic Resonance in Medicine* (see Appendix C).

5.2 Two Reference RIGR (TRIGR)

The Two Reference RIGR (TRIGR) method is motivated by the consideration that, in some applications such as contrast-enhanced imaging, the dynamic process can change the image appearance such that the reference is not a good constraint for image reconstruction. In this case, it is desirable to build information about the dynamic changes into the basis functions. Accordingly, we reconstruct an image of the dynamic changes rather than the dynamic image itself. An additional benefit of this modification is that

the generalized-series parameters need only represent the dynamic changes and not the static parts of the image.

The TRIGR method uses the data acquisition scheme illustrated in Fig. 2. A high-resolution baseline reference data set is acquired where the number of phase encodings is dictated by the spatial resolution requirements. This is followed by a series of reduced dynamic encodings, where the number of encodings is chosen to give the desired temporal resolution. At an appropriate time in the experiment, a high-resolution active reference data set is acquired. In the case of contrast-enhanced dynamic imaging of the breast, the baseline reference would be a high-resolution pre-contrast image. The active reference would be a high-resolution post-contrast image, taken after the dynamic imaging period when the contrast agent is strongly visible in the slice.

The dynamic images are reconstructed using the generalized series model as with the original RIGR algorithm except that information about the dynamic changes is built into the basis functions by using a difference reference image. Specifically, the reconstruction steps are:

1. Construct the difference reference image by subtracting the full active and baseline data sets and reconstructing using the traditional Fourier method.

2. Create the dynamic difference data as

$$d_{\text{diff}}(x) = d_{\text{dyn}}(k) - \hat{d}_{\text{baseline}}(k) \tag{11}$$

   where $d_{\text{dyn}}(k)$ is the dynamic data and $\hat{d}_{\text{baseline}}(k)$ represents the corresponding baseline reference encodings.

3. The TRIGR model is then

$$I_{\text{diff}}(x) = I_{\text{ref}}(x) \sum_{n=-N/2}^{N/2-1} c_n e^{i2\pi n \Delta k x} \tag{12}$$

   where $I_{\text{ref}}(x)$ is the difference reference image of step 1 and N is the number of dynamic encodings. The coefficients c_n are obtained by enforcing data consistency between the reconstructed image and the difference data of Eq. (11), resulting in the equation (47)

$$d_{\text{diff}}(m) = \sum_{n=-N/2}^{N/2-1} c_n d_{\text{ref}}(m-n) \tag{13}$$

where $d_{\text{ref}}(m-n)$ is the difference data created by subtracting the baseline and active reference data sets. Using these coefficients in Eq. 12 will yield the reconstructed dynamic difference image.

4. Many times, the dynamic changes are the items of interest. However, if the dynamic image itself is desired, it can be generated by adding the complex dynamic difference image of step 3 to the baseline reference image, i.e.,

$$I_{\text{dyn}}(x) = I_{\text{baseline}}(x) \quad + \quad I_{\text{diff}}(x) \tag{14}$$

where $I_{\text{baseline}}(x)$ is reconstructed using the standard Fourier technique with the full set of encodings.

The performance of TRIGR has been investigated using additional data sets such as the contrast-enhanced dynamic imaging study of a rat with a large breast tumor shown in Fig. 8. Data for this study was provided by Dr. Erik Wiener. Images (a) and (b) show the reference and dynamic images, respectively, and image (c) is the difference between them. This is the image we are trying to reproduce. These three images were reconstructed from high-resolution data sets of 256 phase encodings using the standard Fourier reconstruction technique. Images (d)-(f) show the difference image reconstructed using 8 dynamic encodings with Keyhole, RIGR and TRIGR, respectively. In the TRIGR image, note the improved delineation of the internal details of the tumor.

A manuscript on the TRIGR technique was published in the July 1996 edition of *Magnetic Resonance in Medicine* (see Appendix B).

5.3 RIGR with Explicit Edge Constraints

In the original RIGR method, dynamic information is only in the generalized-series coefficients. To improve the reconstruction, it would be desirable to also have dynamic information in the generalized-series basis functions which are currently derived solely from the reference image. However, we do not want to lose the high-resolution information available in the reference image. Therefore, this research project aims to use the edge information from the reference image and the contrast information from the dynamic data sets to improve the resulting dynamic images.

To do this, there are two areas which need to be addressed: the extraction of the edge information and the incorporation of this information along with the dynamic contrast information into the generalized-series basis functions. In the first year of this fellowship, the multiresolution edge detection method developed by Ahuja et al (59,60) was selected for the edge extraction step. However, we had difficulty incorporating this information into the generalized-series basis functions. As of the end of the first fellowship year, we had tried using a boxcar model to fit the dynamic data to the regions defined by the reference image edges. The result was used in several ways to modify the RIGR reference image, but no satisfactory method was found.

During the second fellowship year, we addressed both the fitting step and the incorporation of the resulting information into the reference image. To do this, several other models were tested for fitting the dynamic information to the regions defined by the selected reference edges. The Haar wavelet and a higher order Daubechies wavelet (D20) were tried, but the results were unsatisfactory for different reasons in each case. The Haar wavelet fitting maintained the sharp edges of the regions. Unfortunately, the truncation artifact of the Haar wavelet basis set resulted in additional sharp edges inside the regions which could look like features in a reconstructed image and possibly lead to a diagnosis error. The Daubechies wavelet did not have this problem, but the sharp edges of the regions were lost. Since the boxcar results of the previous year showed promise, but indicated that a higher order model may give better results, the localized polynomial approximation (LPA) (61) method was tried which fits a polynomial model to each region.

In addition, the proposed method borrows a strategy from TRIGR and fits the difference of the dynamic data and the corresponding encodings of the reference data set to the regions defined by the selected reference image edges. The result is a fitted image of the dynamic change between the reference and dynamic images. The benefit of this is that the LPA fitting need only represent the change in contrast and not the static parts of the image. This allows the use of a low order (we used up to quadratic) LPA model in the regions.

In summary, the steps of the proposed method are

1. Extract the "most important" reference edges using the multiresolution edge de-

tection method.

2. Create the difference data between the dynamic data and the corresponding encodings of the reference data set.

3. Fit the result of step 2 to the regions defined by the edges selected in step 1 using an LPA model.

4. Add the result of step 3 to the reference image to create a new reference image.

5. Input the new reference image and the dynamic data into the RIGR algorithm to reconstruct the desired dynamic image.

This method was applied to the breast simulation model. Shown in Fig. 9(a) and (b) are the reference and dynamic images, respectively, reconstructed using 128 phase encodings. Image (c) is the new reference image created from the fitted dynamic change image and the reference image (i.e., the result of step 4 above). Images (d)-(f) show the dynamic image reconstructed using the zeropadded Fourier method, the original RIGR, and RIGR with edge constraints, respectively.

Profiles through the upper set of lesions in these images are shown in Fig. 10. Note that, with this image and using 32 encodings, the original RIGR method does not perform much better than the zeropadded Fourier method. However, the RIGR with edge constraints does a much better job at reproducing the lesion profile.

However, if we look at the profiles through the lower set of lesions in Fig. 11, the results from the new technique do not look better than those from the zeropadded Fourier method or the original RIGR method. The reason for this is that the reference image (a) does not contain any information about these lesions. For this reason, the edge detection step cannot extract edges for those lesions, and therefore the fitting step cannot reproduce the contrast changes between the reference and dynamic images. This suggests that incorporating edge information with the TRIGR method could be even more beneficial since the active reference image could be used for the edge extraction step (see next section).

5.4 TRIGR with Explicit Edge Constraints

The TRIGR technique already has information about the dynamic changes in the basis functions. However, perhaps the reconstruction could be improved even further if additional dynamic information were injected using explicit edge constraints. Our initial work indicates that the images will be improved by using this additional information.

To incorporate edge information with TRIGR, the following steps are proposed:

1. Create a difference reference image by subtracting the active and baseline reference data sets and reconstructing using the standard Fourier reconstruction method.
2. Extract the "most important" edges from this difference reference image using the multiresolution edge detection method.
3. Create the difference data by subtracting the dynamic data from the corresponding encodings of the active reference data.
4. Fit the result of step 3 to the regions defined by the edges selected in step 2 using an LPA model.
5. Subtract the result of step 4 from the active reference image to create a new active reference image.
6. Input the baseline reference data, the new reference data created in step 5 and the dynamic data into the TRIGR algorithm.

The result of the application of this technique to the contrast-enhanced breast simulation is shown in Fig. 12. Images (a) and (b) are the baseline reference and dynamic images, respectively, reconstructed using 128 phase encodings. Image (c) is the new active reference created by subtracting the fitted LPA image from the original active reference image. Images (d)-(f) are the dynamic image reconstructed using 32 encodings with the zeropadded Fourier method, the original TRIGR method and the TRIGR with edge constraints method, respectively. Profiles through the upper and lower set of lesions are shown in Figs. 13 and 14, respectively.

As expected, the TRIGR with edge constraints method does a better job than the RIGR with edge constraints method on the lower set of lesions (compare Fig. 14(f) and Fig. 11(f)). However, it is interesting to note that it also performs better on the profile through the upper set of lesions. The TRIGR with edge constraints method profile (Fig. 13(f)) has less ringing than the corresponding profile from the RIGR with edge constraints method (Fig. 10(f)).

6 Conclusions

Based on our study of non-Fourier encoding, we concluded that the current SVD encoding method biases the results towards reproducing the known features in the reference image. As such, it has a reduced capability to capture new features or contrast changes in existing image structures. Therefore, it is not appropriate for application to dynamic imaging.

We developed a method which uses the edge information from a high-resolution reference image and the contrast information from a reduced encoding dynamic data set to create the generalized-series basis functions. With RIGR, this improves the reconstruction of features which are present in the reference image. However, it cannot help the reconstruction of new features which arise during the dynamic imaging period. For this reason, edge constraints were incorporated into the TRIGR method since, in that case, the active reference could be used for the edge extraction step. The reconstruction of new features which arise due to the dynamic process could thus be improved.

In addition, this fellowship has helped me progress in my academic training. Besides the conference presentations and journal papers that have been produced from this research project, I recently passed my preliminary examination. If everything goes as planned, I should complete the requirements for my Ph.D. by the end of this fellowship year.

References

[1] S. H. Heywang, A. Wolf, E. Pruss, T. Hilbertz, W. Eiermann, W. Permanetter, MR imaging of the breast with Gd-DTPA: Use and limitations. *Radiology* **171**, 95–103 (1989).

[2] W. A. Kaiser, MR imaging examination of both breasts within 6 minutes: Technique and first results, in "Proc., RSNA, 75th Annual Meeting, Chicago, 1989", p. 164.

[3] W. A. Kaiser, MR imaging of the breast: Optimal imaging technique, results, limitations and histopathologic correlation, in "Proc., RSNA, 75th Annual Meeting, Chicago, 1989", p. 230.

[4] W. A. Kaiser, O. Mittelmeier, Breast-tissue differentiation by MRI: Results of 361 examinations in 5 years, in "Tissue Characterization in MR Imaging, Springer-Verlag, 1990", pp. 254–257.

[5] W. A. Kaiser, MRM promises earlier breast cancer diagnosis. *Diagnostic Imaging*, 88–93 (1992).

[6] S. E. Harms, D. P. Flamig, K. L. Hesley, W. P. Evans, Magnetic resonance imaging of the breast. *Magn. Reson. Quart.* **8**, 139–155 (1992).

[7] S. E. Harms, D. P. Flamig, Breast: visualizing Ca not seen by radiography. *Body MRI*, 20–24 (1993).

[8] S. E. Harms, D. P. Flamig, MR imaging of the breast. *J. Magn. Reson. Imag.* **3**, 277–283 (1993).

[9] J. P. Stack, O. M. Redmond, M. B. Codd, P. A. Dervan, J. T. Ennis, Breast disease: Tissue characterization with Gd-DTPA enhancement profiles. *Radiology* **174**, 491–494 (1990).

[10] N. M. Hylton, S. D. Frankel, L. J. Esserman, K. Moore, E. Sickles, High resolution 3D maps of contrast enhancement patterns in breast tumors, in "Proc., Soc. Magn. Reson., 3rd Annual Meeting, Nice, France, 1995", p. 439.

[11] F. Kelcz, G. E. Santyr, G. O. Cron, Incorporation of washin and washout criteria for improvement of specificity in dynamic Gadolinium-enhanced MRI of breast lesions, in "Proc., Soc. Magn. Reson., 3rd Annual Meeting, Nice, France, 1995", p. 435.

[12] W. A. Kaiser, E. Zeitler, MR imaging of the breast: Fast imaging sequences with and without Gd-DTPA, preliminary observations. *Radiology* **170**, 681–686 (1989).

[13] B. A. Porter, J. P. Smith, MRI enhances breast cancer detection and staging. *MR*, 18–26,35 (1993).

[14] J. B. Weaver, D. M. Healy, Jr., New MRI acquisition techniques using the window Fourier transforms and the wavelet transforms, in "Proc. Soc. Magn. Reson. Med. 9th Ann. Meeting, New York, NY, 1990", p. 414.

[15] J. B. Weaver, Y. Xu, D. Crean, D. M. Healy, Wavelet encoding in MR imaging, in "Proc., Soc. Magn. Reson. Med., 10th Annual Meeting, 1991", p. 182.

[16] J. B. Weaver, Y. Xu, D. Crean, D. M. Healy, Imaging times in window Fourier transform imaging, in "Proc., Soc. Magn. Reson. Med., 10th Annual Meeting, 1991", p. 857.

[17] D. M. Healy, J. B. Weaver, Two applications of wavelet transforms in magnetic resonance imaging. *IEEE Trans. Info. Theory* **38**, 840–860 (1992).

[18] X. Hu, A. H. Tewfik, H. Garnaoui, A new wavelet based MR imaging technique, in "Proc., Soc. Magn. Reson. Med., 11th Annual Meeting, 1992", p. 432.

[19] L. P. Panych, P. D. Jakab, F. A. Jolesz, Progress towards real-time adaptive imaging using wavelet transform encoding, in "Proc. Soc. Magn. Reson. Med. 11th Ann. Meeting, Berlin, Germany, 1992", p. 4513.

[20] L. P. Panych, P. D. Jakab, Wavelet encoding in the section-select dimension, in "Proc. Soc. Magn. Reson. Imag. 10th Ann. Meeting, New York, NY, 1992", p. 90.

[21] J. B. Weaver, Y. Xu, D. M. Healy, J. R. Driscoll, Wavelet-encoded MR imaging. *Magn. Reson. Med.* **24**, 275–287 (1992).

[22] J. B. Weaver, D. M. Healy, Jr., D. Crean, Y. Xu, Wavelet encoding with smooth wavelets: Short RF pulses, in "Proc. Soc. Magn. Reson. Med. 11th Ann. Meeting, Berlin, Germany, 1992", p. 4264.

[23] J. B. Weaver, D. M. Healy, Jr., Y. Xu, SNR for wavelet encoded MR, in "Proc. Soc. Magn. Reson. Med. 11th Ann. Meeting, Berlin, Germany, 1992", p. 3822.

[24] J. B. Weaver, D. M. Healy, Jr., Adaptive wavelet encoding in cardiac imaging, in "Proc. Soc. Magn. Reson. Med. 11th Ann. Meeting, Berlin, Germany, 1992", p. 3906.

[25] J. M. Hanson, Z.-P. Liang, P. C. Lauterbur, A new method for fast dynamic imaging using wavelet transforms, in "Proc., Soc. Magn. Reson. Med., 12th Annual Meeting, 1993", p. 712.

[26] K. Oshio, L. P. Panych, F. A. Jolesz, Wavelet encoded MR imaging (implementation), in "Proc. Soc. Magn. Reson. Med. 12th Ann. Meeting, New York, NY, 1993", p. 1213.

[27] L. P. Panych, P. D. Jakab, F. A. Jolesz, An implementation of wavelet-encoded MR imaging, in "Proc., Soc. Magn. Reson. Imag., 11th Annual Meeting, 1993", p. 26.

[28] L. P. Panych, P. D. Jakab, F. A. Jolesz, Implementation of wavelet-encoded MR imaging. *J. Magn. Reson. Imag.* **3**, 649–655 (1993).

[29] R. D. Peters, M. L. Wood, Practical considerations for the implementation of wavelet encoding in MRI, in "Proc. Soc. Magn. Reson. Med. 12th Ann. Meeting, New York, NY, 1993", p. 1212.

[30] L. P. Panych, F. A. Jolesz, A dynamically adaptive imaging algorithm for wavelet-encoded MRI. *Magn. Reson. Med.* **32**, 738–748 (1994).

[31] L. P. Panych, F. A. Jolesz, Theoretical comparison of resolution in wavelet and Fourier encoded MR images, in "Proc., Soc. Magn. Reson., 2nd Annual Meeting, San Francisco, 1994", vol. 2, p. 776.

[32] L. P. Panych, F. A. Jolesz, Design of optimal wavelet bases for wavelet encoded MRI, in "Proc., Soc. Magn. Reson., 2nd Annual Meeting, San Francisco, 1994", vol. 2, p. 777.

[33] N. Gelman, M. L. Wood, R. D. Peters, Three dimensional gradient echo imaging using wavelet encoding, in "Proc. Soc. Magn. Reson. 3rd Ann. Meeting, Nice, France, 1995", p. 662.

[34] R. D. Peters, M. L. Wood, Multilevel wavelet-encoded MR imaging, in "Proc. Soc. Magn. Reson. 3rd Ann. Meeting, Nice, France, 1995", p. 194.

[35] N. Gelman, M. L. Wood, Wavelet encoding for improved SNR and retrospective slice thickness adjustment, in "Proc. Int. Soc. Magn. Reson. Med. 4th Ann. Meeting, New York, NY, 1996", p. 1535.

[36] W.-L. Hwang, N.-K. Chen, C. Chen, H. N. Yeung, Application of wavelet decomposition in dynamic MRI, in "Proc. Int. Soc. Magn. Reson. Med. 4th Ann. Meeting, New York, NY, 1996", p. 1650.

[37] L. P. Panych, Theoretical comparison of Fourier and wavelet encoding in magnetic resonance imaging. *IEEE Trans. Med. Imaging* **15**, 141–153 (1996).

[38] R. D. Peters, M. L. Wood, Multilevel wavelet-transform encoding in MRI. *J. Magn. Reson. Imag.* **6**, 529–540 (1996).

[39] Y. Cao, D. N. Levin, On the relationship between feature-recognizing MRI and MRI encoded by singular value decomposition. *Magn. Reson. Med.* **33**, 140–142 (1995).

[40] Y. Cao, D. N. Levin, L. Yao, Locally focused MRI. *Magn. Reson. Med.* **34**, 858–867 (1995).

[41] L. P. Panych, C. Oesterle, G. P. Zientara, J. Hennig, Implementation of a fast gradient-echo SVD encoding technique for dynamic imaging, in "Proc. Soc. Magn. Reson. 3rd Ann. Meeting, Nice, France, 1995", p. 663.

[42] L. P. Panych, C. Oesterle, G. P. Zientara, J. Hennig, Implementation of a fast gradient-echo SVD encoding technique for dynamic imaging. *Magn. Reson. Med.* **35**, 554–562 (1995).

[43] P. Saiviroonporn, G. P. Zientara, L. P. Panych, F. A. Jolesz, Real-time computations for dynamically adaptive SVD encoded MRI, in "Proc. Soc. Magn. Reson. 3rd Ann. Meeting, Nice, France, 1995", p. 665.

[44] G. P. Zientara, L. P. Panych, F. A. Jolesz, Dynamically adaptive MRI with encoding by singular value decomposition. *Magn. Reson. Med.* **32**, 268–274 (1994).

[45] G. P. Zientara, L. P. Panych, F. A. Jolesz, Keyhole SVD encoded MRI, in "Proc. Soc. Magn. Reson. 2nd Ann. Meeting, San Francisco, CA, 1994", p. 778.

[46] G. P. Zientara, L. P. Panych, F. A. Jolesz, Lanczos spatial encodings for dynamically adaptive MRI, in "Proc. Soc. Magn. Reson. 3rd Ann. Meeting, Nice, France, 1995", p. 664.

[47] Z.-P. Liang, P. C. Lauterbur, Improved temporal/spatial resolution in functional imaging through generalized series reconstruction, in "Works-in-Progress Proc. Soc. Magn. Reson. Imag. 10th Ann. Meeting, New York, NY, 1992", p. S15.

[48] Z.-P. Liang, P. C. Lauterbur, An efficient method for dynamic magnetic resonance imaging. *IEEE Trans. Med. Imaging* **13**, 677–686 (1994).

[49] J. J. van Vaals, H. H. Tuithof, W. T. Dixon, Increased time resolution in dynamic imaging, in "Proc. Soc. Magn. Reson. Imag. 10th Ann. Meeting, New York, NY, 1992", p. 44.

[50] J. E. Bishop, I. Soutar, W. Kucharczyk, D. B. Plewes, Rapid sequential imaging with shared-echo fast spin-echo MR imaging, in "Works-in-Progress Proc. Soc. Magn. Reson. Imag. 10th Ann. Meeting, New York, NY, 1992", p. S22.

[51] D. B. Plewes, J. Bishop, I. Soutar, E. Cohen, Errors in quantitative dynamic three-dimensional Keyhole MR imaging of the breast. *J. Magn. Reson. Imag.* **5**, 361–364 (1995).

[52] D. E. Egerter, Keyhole imaging enhances dynamic contrast studies. *MR*, 8,13,49 (1992).

[53] X. Hu, On the "keyhole" technique. *J. Magn. Reson. Imag.* **4**, 231 (1994).

[54] T. A. Spraggins, Simulation of spatial and contrast distortions in keyhole imaging. *Magn. Reson. Med.* **31**, 320–322 (1994).

[55] J. Bishop, R. M. Henkelman, D. B. Plewes, Dynamic spin-echo imaging: Theoretical assessment and implementation. *J. Magn. Reson. Imag.* **4**, 843–852 (1994).

[56] J. M. Hanson, Z.-P. Liang, R. L. Magin, J. L. Duerk, P. C. Lauterbur, A comparison of RIGR and SVD dynamic MRI methods, in "Proc. Int. Soc. Magn. Reson. Med. 4th Ann. Meeting, New York, NY, 1996", p. 118.

[57] J. M. Hanson, Z.-P. Liang, R. L. Magin, J. L. Duerk, P. C. Lauterbur, A comparison of RIGR and SVD dynamic MRI methods. *Magn. Reson. Med.* ?, ? (submitted April 1996).

[58] G. H. Golub, C. F. Van Loan, "Matrix Computations", 2nd ed., John Hopkins University Press, Baltimore, MD, 1989.

[59] N. Ahuja, A transform for detection of multiscale image structure, in "Proc., DARPA Image Understanding Workshop, 1993", pp. 893–902.

[60] N. Ahuja, A transform for detection of multiscale image structure, in "Proc., Comp. Vision Patt. Recog., New York, 1993", pp. 780–781.

[61] Z.-P. Liang, Constrained reconstruction from incomplete and noisy data: A new parametric approach, Ph.D. thesis, Case Western Reserve University, Cleveland, 1989", Department of Biomedical Engineering.

7 Appendix A - Conference Presentation

A Comparison of RIGR and SVD Dynamic MRI Methods

J.M. Hanson, Z.-P. Liang, R.L. Magin, J.L. Duerk* and P.C. Lauterbur
Department of Electrical and Computer Engineering, University of Illinois at Urbana-Champaign, Urbana, Illinois
*Departments of Radiology and Biomedical Engineering, Case Western Reserve University, Cleveland, Ohio

Introduction

In dynamic MR imaging, a sequence of images of a given slice or volume is acquired to monitor a process such as the insertion of a biopsy needle. In such an application, it is necessary to have high spatial and temporal resolution to adequately monitor the process. Three methods which have been proposed to improve the temporal resolution of a sequence of dynamic images are Reduced-encoding Imaging by Generalized-series Reconstruction (RIGR) [1], Singular Value Decomposition (SVD) [2], and Keyhole-SVD methods (KSVD) [3]. The common thread in these methods is the acquisition of a single high-resolution reference data set followed by a series of reduced dynamic encodings. The differences arise in the choice of the dynamic encodings and the reconstruction procedure for the dynamic images. In this paper, the performance of the RIGR, KSVD and SVD methods for dynamic MR imaging is compared using computer simulation.

Method

To simulate the RIGR data acquisition, k-space data sets, including d_{ref}, were generated from a sequence of high-resolution images. The central phase encodings were used as the dynamic phase encodings, d_{dyn},. For the SVD methods, the singular value decomposition of the reference image was calculated as

$$I_{\text{ref}} = U \Sigma V^H \tag{1}$$

where U, Σ and V are the matrices containing the left singular vectors, singular values and right singular vectors, respectively. The left singular vectors u_i corresponding to the largest L singular values were selected as excitation profiles or *eigenencodings* for the dynamic images. For a dynamic image I_{dyn}, data were generated by

$$S_{\text{dyn}} = U_L^H I_{\text{dyn}} \tag{2}$$

where U_L is the matrix constructed from the L selected left singular vectors. For the KSVD method, the reference image information was included in the reconstruction as

$$I_{\text{ref},N-L} = U_{N-L}^H \Sigma_{N-L} V^H \tag{3}$$

where U_{N-L} and Σ_{N-L} are truncated matrices consisting of the $N-L$ least significant left singular vectors and singular values, respectively. The following equations were used for image reconstruction:

$$\text{SVD:} \quad \hat{I}_{\text{dyn}} = U_L S_{\text{dyn}} \tag{4}$$

$$\text{KSVD:} \quad \hat{I}_{\text{dyn}} = U_L S_{\text{dyn}} + U_{N-L}^H \Sigma_{N-L} V^H \tag{5}$$

$$\text{RIGR:} \quad \hat{I}_{\text{dyn}} = I_{\text{ref}} \textstyle\sum_n c_n e^{i2\pi n \Delta k x} \tag{6a}$$

$$\text{where } d_{\text{dyn}}(m) = \textstyle\sum_n c_n d_{\text{ref}}(m-n) \tag{6b}$$

Results and Discussion

Illustrated in Fig. 1 is a frame from a simulated needle biopsy procedure in which the needle motion was parallel to the frequency encoding direction. Since the reference image contains no information about the needle, the simulation tests the ability of the methods to discover new features which are the objects of interest in dynamic imaging. Figs. 1(a-b) show the reference and dynamic images, respectively, reconstructed with 256 phase encodings using the standard Fourier method. Figs. 1(c-f) show the dynamic image reproduced with 32 dynamic encodings using SVD, KSVD, truncated Fourier transform and RIGR, respectively. The RIGR images also had less artifacts than the SVD and KSVD images when the needle motion was perpendicular to the frequency encoding direction.

In RIGR, the dynamic encodings are not optimized with respect to the reference image and are typically collected at the center of k-space. If the number of dynamic encodings collected is small or if the dynamic changes introduce new edges that are not present in the reference image, Gibbs ringing will result from these features as is evident in Fig. 1(f). However, RIGR faithfully depicts the center of the needle (arrow indicates needle center). This is not the case with the SVD images in Figs. 1(c-d), in which the needle appears displaced from the correct location. With the SVD methods, the "excitation" is biased towards reproducing the dominant features in the reference image, thus reducing its capability to capture new features. Although the selected eigenencodings are optimal for the reference image, they are not necessarily optimal, or even good, basis functions for the dynamic images.

In addition, KSVD suffers from the same data inconsistency problem that can occur with regular Keyhole which is illustrated here with a contrast-enhanced imaging simulation. Figures 2(a-b) are the reference and dynamic images, respectively, reconstructed using the standard Fourier method with 128 phase encodings. Figures 2(c-d) show the dynamic image reconstructed with 8 dynamic encodings using KSVD and RIGR, respectively. Note the artifacts due to data inconsistency between the reference and dynamic data in Fig. 2(c). With RIGR, data consistency is ensured through the fitting step in Eq. 6b.

In these simulations, it was assumed that the eigenencodings for the SVD methods could be exactly excited. However, this is difficult to achieve in practice, and deviations from ideal excitation degrade the reconstructed image [2]. This is not a concern with RIGR since conventional phase encoding is used.

Conclusions

Our study shows that RIGR is superior to SVD in capturing new features which arise due to contrast enhancement, functional changes, intervention or other means.

Acknowledgements

This work is supported by Army Grant DAMD17-94-J-4126, NSF grants NSF-BES-95-02121 and NSF-MIP-94-10463 and the Beckman Institute.

References

[1] Z.-P. Liang, et al, *10th SMRI*, S15, 1992.
[2] G.P. Zientara, et al, *MRM* 32, 268-274, 1994.
[3] G.P. Zientara, et al, *2nd SMR*, 778, 1994.

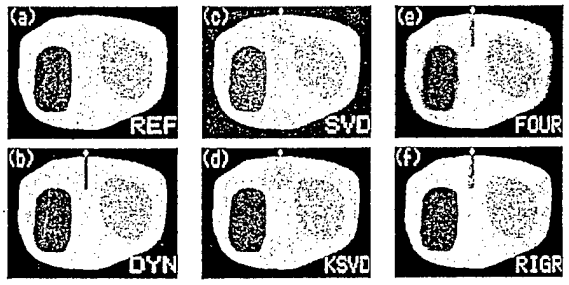

Figure 1: Simulation of needle biopsy procedure

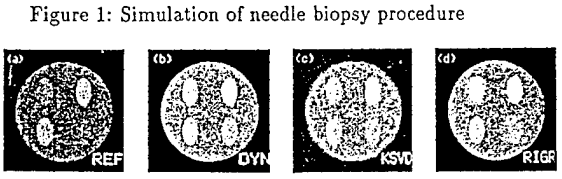

Figure 2: Illustration of KSVD data inconsistency

8 Appendix B - Published Manuscript

Fast Dynamic Imaging Using Two Reference Images

Jill M. Hanson, Zhi-Pei Liang, Erik C. Wiener, Paul C. Lauterbur

This paper presents a fast dynamic imaging method which is characterized by the acquisition of two high-resolution reference images and a sequence of low-resolution dynamic data sets. Image reconstruction is accomplished using a generalized series based algorithm. Experimental results demonstrate that dynamic images with high temporal resolution can be obtained while maintaining excellent spatial resolution. This method will be useful for a variety of dynamic imaging applications including contrast-enhanced dynamic imaging and functional brain studies.

Key words: dynamic imaging; fast imaging; image reconstruction; generalized series.

INTRODUCTION

Many MRI applications such as contrast-enhanced dynamic imaging and functional brain studies involve the collection of a time series of images of the same slice or volume to monitor a dynamic process. To capture the details of the dynamic process, it is important to obtain high temporal resolution while maintaining high spatial resolution. However, with conventional Fourier imaging, the requirements for increased time resolution and spatial resolution are conflicting. Since each of the dynamic images is acquired independently, the temporal resolution possible is limited by the number of spatial encodings applied.

Two methods that have recently been proposed for improving the temporal resolution of a sequence of dynamic images are Reduced-encoding Imaging through Generalized-series Reconstruction (RIGR) (1–5) and Keyhole (6–13). The techniques are similar in that they both acquire a single high-resolution reference image with a series of reduced dynamic encodings. However, Keyhole uses a Fourier transform based approach for the reconstruction of the dynamic images. The high frequency data from the reference image is simply pasted onto the low-resolution dynamic encodings to create a full data set. This data set is then inverse Fourier transformed to arrive at the dynamic image. Image artifacts can occur as a result of data inconsistency between the reference and dynamic data sets. In addition, Keyhole can only reconstruct a low-resolution version of the dynamic changes (14, 15). On the other hand, the RIGR algorithm uses the generalized series model to reconstruct the dynamic images. Information from the reference image is built into the basis functions of the model, which allows it to track the dynamic process with greater resolution than is possible using Fourier reconstruction techniques with an equivalent number of dynamic encodings. This paper presents a modified RIGR technique that uses the additional information from a second reference image to improve spatial and temporal resolution in the dynamic images. (For a complete description of the original RIGR technique, the reader is referred to (4)).

METHOD

Compared with the original RIGR method, the proposed method is characterized by two distinguishing features: (1) the collection of two reference data sets and (2) the application of the generalized series model to the difference data sets, resulting in direct reconstruction of the dynamic signal variations. This method is motivated by the consideration that, in many dynamic imaging applications, it is possible to obtain two high-resolution reference images: one for the "baseline" state and another for the "active" state. In the example of contrast-enhanced dynamic imaging of breast cancer, where the aim is to track the changes that occur in the breast for several minutes following the injection of a contrast agent, the baseline reference would be a high-resolution precontrast image. The active reference would be a high-resolution postcontrast image taken after the dynamic data sets when the contrast agent is strongly visible in the image.

Data acquisition for the proposed method is characterized by the following three steps:

1. Acquire a high-resolution baseline reference image where the number of phase encodings is chosen to satisfy the spatial resolution requirements.
2. Acquire a series of low-resolution dynamic data sets where the number of phase encodings per set is chosen to give the desired temporal resolution.
3. Acquire a high-resolution active reference image. Note that this image can be acquired in the middle of the dynamic encodings if that is better for a given application. All that is required is that the active reference image indicate the areas of change from the baseline reference image. In some situations, it may be preferable to obtain reference images at various points during the experimental procedure and then use the appropriate two reference images for each dynamic image.

Reconstruction of the dynamic images is accomplished using the generalized series model with a reference im-

MRM 36:172–175 (1996)

From the Biomedical Magnetic Resonance Laboratory, Electrical and Computer Engineering Department (J.M.H., Z-P.L., P.C.L.), Beckman Institute for Advanced Science and Technology, University of Illinois at Urbana-Champaign, Urbana, Illinois.

Address correspondence to: Paul C. Lauterbur, Ph.D., Biomedical Magnetic Resonance Laboratory, University of Illinois at Urbana-Champaign, 1307 West Park Street, Urbana, IL 61801.

Received July 13, 1995; revised December 11, 1995; accepted February 15, 1996.

This work was supported in part by Army Grant DAMD17-94-J-4126 (JMH), NIH Grant PHS-5-P41-RR05964, NSF-MIP-94-10463-RIA Award, the National Center for Supercomputing Applications, the Beckman Institute, the Servants United Foundation, and the Whitaker Foundation.

The content of this paper does not necessarily reflect the position or the policy of the government, and no official endorsement should be inferred.

0740-3194/96 $3.00

age reflecting the areas of change in the sequence of images. Specifically, the reconstruction steps are:

1. Construct the difference reference image by reconstructing the baseline and active reference images using the traditional Fourier method with the full set of encodings and subtracting the complex images.
2. Create the dynamic difference data by subtracting from the dynamic data the corresponding encodings of the baseline reference image, namely

$$d_{\text{diff}}(k) = d_{\text{dyn}}(k) - \hat{d}_{\text{baseline}}(k) \quad [1]$$

where $d_{\text{dyn}}(k)$ is the dynamic data and $\hat{d}_{\text{baseline}}(k)$ represents the corresponding part of the baseline reference encodings.
3. The RIGR model then becomes:

$$I_{\text{diff}}(x) = |I_{\text{ref}}(x)| \sum_{n=-N/2}^{N/2-1} c_n e^{i2\pi n\Delta kx} \quad [2]$$

where $I_{\text{ref}}(x)$ is the difference reference image of step 1 and N is the number of dynamic encodings. The coefficients c_n are obtained by fitting the difference data of Eq. [1] to the following equation to maintain data consistency (1)

$$d_{\text{diff}}(m) = \sum_{n=-N/2}^{N/2-1} c_n d_{\text{ref}}(m-n) \quad [3]$$

where $d_{\text{ref}}(m-n)$ is the difference data created by subtracting the baseline and active reference data sets. Plugging these coefficients into Eq. [2] will yield the reconstructed dynamic difference image.
4. If the dynamic image itself is desired, it can be generated by adding the complex dynamic difference image of Step 3 to the baseline reference image, ie:

$$I_{\text{dyn}}(x) = I_{\text{baseline}}(x) + I_{\text{diff}}(x) \quad [4]$$

where $I_{\text{baseline}}(x)$ is reconstructed using the standard Fourier technique with the full set of encodings.

RESULTS

The method was tested on contrast-enhanced dynamic MR imaging of rats with breast cancer. A rat with a very large breast tumor was imaged using a spin echo sequence (*TR* 300/*TE* 20). A high-resolution precontrast reference image was obtained. The contrast agent was then injected, and a series of dynamic images was acquired. This was followed by a high-resolution postcontrast image. To simulate the reduced encoding acquisition strategy used by Keyhole, the original RIGR method and the proposed method, the central encodings were used for the reconstruction of the dynamic images by these methods.

A line drawing of a representative transverse slice through the tumor is shown in Fig. 1. Various anatomical features are identified in addition to the tumor. The images corresponding to this line drawing are shown in

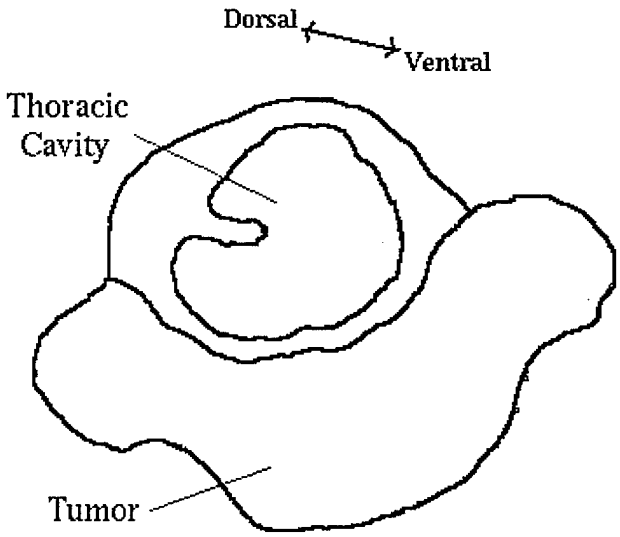

FIG. 1. Line drawing of the transverse rat slice shown in Fig. 2.

Fig. 2. The precontrast and postcontrast reference images that were reconstructed using the standard Fourier method with 256 phase encodings are illustrated in Figs. 2a and 2b, respectively. Image 2c shows the dynamic difference image between the dynamic image (not shown) and the baseline reference image and was reconstructed using 256 phase encodings. Images 2d, 2e, and 2f show the dynamic difference image reproduced using only eight dynamic phase encodings with the Keyhole method, the original RIGR method and the two-reference RIGR method, respectively. It can be seen that Fig. 2f more closely reproduces the dynamic changes than either Figs. 2d or 2e. Note in particular the improved delineation of the internal details of the tumor, such as those indicated by the arrows.

DISCUSSION

The generalized series approach that is employed in the proposed method builds information from the reference image into the basis functions of the model. The result is a high-resolution dynamic image since the basis functions are high-resolution. In the original RIGR algorithm, the basis functions were from either the baseline or the active reference image. However, the contrast in these reference images may not accurately reflect the dynamic changes, which could lead to image artifacts. Given that two reference images are available, we can instead build information about the dynamic changes into the basis functions by using a difference reference image. This difference reference image will more closely represent the areas of change and will lead to a better reconstruction of the dynamic changes.

Accordingly, we use the proposed algorithm to reconstruct an image of the dynamic changes rather than the dynamic image itself. (The dynamic image can then be obtained by simply overlaying the dynamic change image on the reference image.) An additional benefit of this modification is that the parameters of the generalized series model need only represent the dynamic changes, not the static parts of the image. This leads to a more

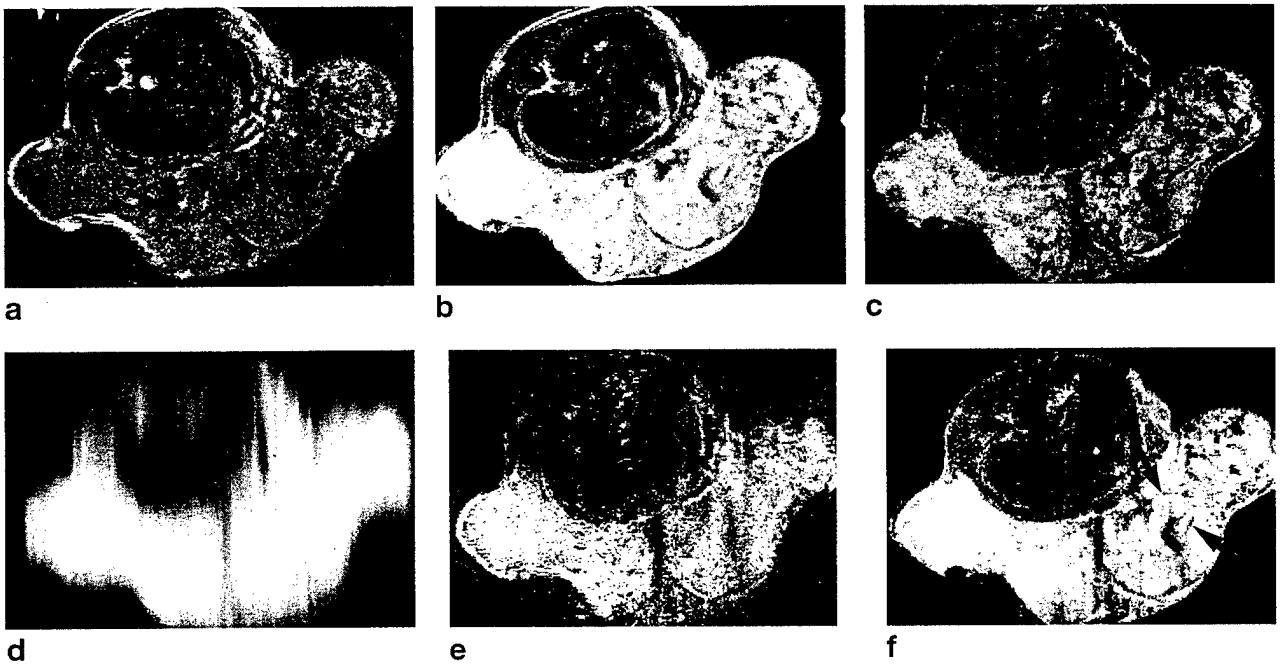

FIG. 2. Images of a rat with breast cancer. (a)–(c) Precontrast reference, postcontrast reference and dynamic difference images, respectively, reconstructed with 256 phase encodings. (d)–(f) Dynamic difference image reproduced using only eight dynamic phase encodings with Keyhole, original RIGR, and two-reference RIGR, respectively. Note in particular the improved delineation of the internal details of the tumor, such as those indicated by the arrows.

faithful representation of the dynamic changes and, thus, a better dynamic image.

These expectations are realized in the experimental results that have been obtained. As shown in Fig. 2, the image reconstructed using the proposed method (Fig. 2f) more closely resembles the desired difference image (Fig. 2c) than either the Keyhole (Fig. 2d) or the original RIGR algorithms (Fig. 2e). Since the proposed method used only eight dynamic phase encodings, as opposed to 256, this would yield a 32-fold time savings compared with standard Fourier imaging with minimal loss of image quality.

One could consider employing a similar methodology with Keyhole by appending the high frequency difference reference data to the low frequency dynamic difference data sets followed by the inverse Fourier transform. Although the resulting difference images will be high resolution, it is easy to prove that the actual dynamic signal changes will still be reconstructed with low resolution. This behavior is similar to the single reference image case analyzed by Spraggins (14) and Hu (15); that is, no benefit is gained from the use of two reference images in this Keyhole scheme.

CONCLUSION

A fast dynamic imaging method that uses two high-resolution reference images and a sequence of reduced dynamic encodings to reconstruct a time series of dynamic images has been developed. The proposed method shows improved quality of the reconstructed dynamic images as compared with both Keyhole and the original RIGR, which would lead to a more faithful tracking of the dynamic processes. The method would be useful for a variety of dynamic imaging applications such as contrast-enhanced dynamic MR imaging and functional brain studies.

ACKNOWLEDGMENTS

The authors thank Carl Gregory for experimental assistance and helpful discussions.

REFERENCES

1. Z.-P. Liang, P. C. Lauterbur, Improved temporal/spatial resolution in functional imaging through generalized series reconstruction, *in* "Proc., SMRI, 10th Annual Meeting, New York, 1992," p. S15.
2. A. Webb, Z.-P. Liang, R. L. Magin, P. C. Lauterbur, Application of a generalized-series reconstruction algorithm to biologic MR imaging, *in* "Proc., SMRI, 10th Annual Meeting, New York, 1992," p. S26.
3. Z.-P. Liang, P. C. Lauterbur, Efficient time-sequential imaging through generalized series modeling: a simulation analysis, *in* "Proc., SMRM, 11th Annual Meeting, Berlin, 1992," p. 4266.
4. Z.-P. Liang, P. C. Lauterbur, An efficient method for dynamic magnetic resonance imaging. *IEEE Trans. Med. Imaging* **13**, 677–686 (1994).
5. A. Webb, Z.-P. Liang, R. L. Magin, P. C. Lauterbur, Application of reduced-encoding MR imaging with generalized-series reconstruction (RIGR). *J. Magn. Reson. Imaging* **3**, 925–928 (1993).
6. J. E. Bishop, I. Soutar, W. Kucharczyk, D. B. Plewes, Rapid sequential imaging with shared-echo fast spin-echo MR imaging, *in* "Proc., SMRI, 10th Annual Meeting, New York, 1992," p. S22.
7. J. J. van Vaals, H. H. Tuithof, W. T. Dixon, Increased time resolution in dynamic imaging, *in* "Proc., SMRI, 10th Annual Meeting, New York, 1992," p. 44.
8. M. E. Brummer, W. T. Dixon, B. Gerety, H. Tuithof, Composite *k*-space windows (keyhole techniques) to improve temporal resolution in a dynamic series of images following contrast administration, *in* "Proc., SMRM. 11th Annual Meeting, Berlin, 1992," p. 4236.

9. R. A. Jones, O. Haraldseth, T. B. Muller, P. A. Rinck, G. Unsgard, A. N. Oksendal, Dynamic, contrast enhanced, NMR perfusion imaging of regional cerebral ischaemia in rats using k space substitution, *in* "Proc., SMRM, 11th Annual Meeting, Berlin, 1992," p. 1138.
10. G. B. Pike, J. O. Fredrickson, G. H. Glover, D. R. Enzmann, Dynamic susceptibility contrast imaging using a gradient-echo sequence, *in* "Proc., SMRM, 11th Annual Meeting, Berlin, 1992," p. 1131.
11. J. J. van Vaals, H. Engels, R. G. de Graaf, H. H. Tuithof, J. A. den Boer, W. T. Dixon, R. C. Nelson, J. L. Chezmar, Method for accelerated perfusion imaging, *in* "Proc., SMRM, 11th Annual Meeting, Berlin, 1992," p. 1139.
12. J. J. van Vaals, M. E. Brummer, W. T. Dixon, H. H. Tuithof, H. Engels, R. C. Nelson, B. M. Gerety, J. L. Chezmar, J. A. den Boer, "Keyhole" method for accelerating imaging of contrast agent uptake. *J. Magn. Reson. Imaging* **3**, 671–675 (1993).
13. R. A. Jones, O. Haraldseth, T. B. Muller, P. A. Rinck, A. N. Oksendal, K-space substitution: a novel dynamic imaging technique. *Magn. Reson. Med.* **29**, 830–834 (1993).
14. T. A. Spraggins, Simulation of spatial and contrast distortions in keyhole imaging. *Magn. Reson. Med.* **31**, 320–322 (1994).
15. X. Hu, On the "keyhole" technique. *J. Magn. Reson. Imaging* **4**, 231 (1994).

9 Appendix C - Submitted Manuscript

A Comparison of RIGR and SVD Dynamic Imaging Methods

Jill M. Hanson, Zhi-Pei Liang, Richard L. Magin, Jeff L. Duerk[†], Paul C. Lauterbur

Biomedical Magnetic Resonance Laboratory, Electrical and Computer Engineering Department, Magnetic Resonance Engineering Laboratory and Beckman Institute for Advanced Science and Technology, University of Illinois at Urbana-Champaign
[†]Departments of Radiology and Biomedical Engineering, Case Western Reserve University, Cleveland, Ohio

Abstract

Several constrained imaging methods have recently been proposed for dynamic imaging applications. This paper compares two of these methods: the Reduced-encoding Imaging by Generalized-series Reconstruction (RIGR) and Singular Value Decomposition (SVD) methods. RIGR utilizes *a priori* data for optimal image reconstruction whereas the SVD method seeks to optimize data acquisition. However, this study shows that the existing SVD encoding method tends to bias the data acquisition scheme towards reproducing the known features in the reference image. This characteristic of the SVD encoding method reduces its capability to capture new image features and makes it less suitable than RIGR for dynamic imaging applications.

1 Introduction

The main challenge with dynamic MRI lies in the requirement of both high temporal and high spatial resolutions. The two avenues of attack on this problem have been fast-scan imaging and reduced-scan imaging. Fast-scan imaging methods seek to acquire a full data set in a time that is short relative to the dynamic processes whereas reduced-scan imaging methods incorporate *a priori* information into the imaging process to reduce the number of dynamic encodings required. Some of the better known reduced-scan techniques are the Reduced-encoding Imaging by Generalized-series Reconstruction (RIGR) method (1), the Keyhole method (2, 3) and the Singular Value Decomposition (SVD) method (4, 5). Since the RIGR and Keyhole methods have been compared previously (1, 6), this paper will focus on a comparison of the RIGR method

with the SVD method. A common feature of these methods is that a high-resolution reference image is obtained prior to the dynamic imaging period. RIGR uses the reference image only to constrain the reconstruction whereas the SVD method uses the reference image to determine the dynamic encodings that are acquired. In this paper, we present a comprehensive evaluation of the performance of these methods with respect to dynamic imaging applications.

2 Method

RIGR is a Fourier-encoding method. For each dynamic image, it collects a reduced set of phase-encoded data in the central region of k-space. The unmeasured dynamic data are estimated using a generalized series model as (1)

$$\hat{I}_{\text{dyn}}(x) = |I_{\text{ref}}(x)| \sum_{n=-N/2}^{N/2-1} c_n \, e^{i2\pi n \Delta k x} \qquad [1]$$

where I_{ref} is the high-resolution reference image, N is the number of dynamic encodings, and Δk is the phase encoding step in k-space. The N model parameters c_n are determined by the constraint that the model-estimated data at all sampled k-space points should be identical to the actual measured data d_{dyn}, which leads to

$$d_{\text{dyn}}(m) = \sum_{n=-N/2}^{N/2-1} c_n \, \hat{d}_{\text{ref}}(m-n) \qquad -N/2 \le m \le N/2-1 \qquad [2]$$

where

$$\hat{d}_{\text{ref}}(m-n) = \int_{-\infty}^{\infty} |I_{\text{ref}}(x)| e^{-i2\pi(m-n)\Delta k x} dx. \qquad [3]$$

Substituting the resulting coefficients into Eq. [1] will yield the desired dynamic image.

The SVD methods use spatially selective RF pulses to acquire a reduced set of "SVD-encoded" dynamic data. Unmeasured data are either set to zero (SVD method) or filled with the reference data (SVD-Keyhole method). SVD synthesis is then used to reconstruct the dynamic image. Specifically, given a reference image I_{ref}, the singular value decomposition of the reference image is first performed as

$$I_{\text{ref}} = U \, \Sigma \, V^H \qquad [4]$$

where U, Σ and V are the matrices containing the left singular vectors u_i, singular values σ_i and right singular vectors v_i, respectively. For SVD encoding along the vertical or horizontal directions, the u_i or v_i, respectively, corresponding to the largest N singular values are selected as RF excitation profiles for the dynamic images. In the pure vertical encoding case, for example, the dynamic data set generated for each dynamic image is the projection of the ideal image I_{dyn} onto the space spanned by the selected left singular vectors. This can be expressed as

$$S_{\text{dyn}} = U_N^H \, I_{\text{dyn}} \qquad [5]$$

where U_N is the matrix constructed from the N selected left singular vectors. To reconstruct the dynamic images, the dynamic data are multiplied by U_N as

$$\hat{I}_{\text{dyn}} = U_N \, S_{\text{dyn}}. \qquad [6]$$

Note that if $N = M$ where M is the number of reference encodings, $\hat{I}_{\text{dyn}} = I_{\text{dyn}}$ because $U_N \, S_{\text{dyn}} = U \, S_{\text{dyn}} = UU^H \, I_{\text{dyn}}$.

A modification of the basic SVD method known as the SVD-Keyhole method (5) uses the same data acquisition scheme. The difference lies in the reconstruction step. For the SVD-Keyhole method, the eigenimage

$$I_{\text{ref},M-N} = U_{M-N} \, \Sigma_{M-N} \, V_{M-N}^H \qquad [7]$$

is formed where U_{M-N}, Σ_{M-N} and V_{M-N} are truncated matrices consisting of the $M-N$ least significant left singular vectors, singular values and right singular vectors, respectively. The final image is obtained by adding $I_{\text{ref},M-N}$ to $\hat{I}_{\text{dyn}}$ given in Eq. [6] such that

$$\hat{\hat{I}}_{\text{dyn}} = U_N \, S_{\text{dyn}} + I_{\text{ref},M-N}. \qquad [8]$$

The methods were compared using computer simulations on both simulated and real high-resolution MRI data. The study was tailored to address the following specific characteristics: (1) the ability to track contrast changes in existing image structures (as calculated by the average signal magnitude in the region of interest) and (2) the ability

to reconstruct novel dynamic image features (as indicated by the appearance of the image features and artifacts). The simulations were carried out with a fixed number of dynamic encodings (i.e., a fixed frame rate) for the RIGR and SVD methods. Note that data acquisition for the RIGR method will require the same amount of time per encoding as a conventional scan. For the SVD method, the acquisition time per encoding will be roughly that of a conventional scan if the dynamic encoding vectors are selected prior to the dynamic imaging period. If the dynamic encoding vectors are selected during the dynamic imaging period based on the preceeding dynamic image, the acquisition time per dynamic image will be increased by the time required to calculate the dynamic encodings. In the simulations, we chose to ignore this extra time for the SVD encoding method.

To simulate the RIGR data acquisition, k-space data sets were generated from a sequence of high-resolution images. A baseline high-resolution data set was used as the reference data, and the central N phase encodings from the remaining data sets were used as the dynamic phase encodings. To simulate the SVD and SVD-Keyhole imaging methods, the singular value decomposition of the reference image was calculated according to Eq. [4]. The dynamic data were then generated using Eq. [5].

To test the performance of the methods in tracking dynamic contrast changes such as those that occur following the injection of a contrast agent, a contrast-enhanced simulation was performed in which all the lesions were visible in the reference image. The simulation was then repeated using real MRI data from a contrast-enhanced study of a rat with breast cancer. To investigate the ability of the methods to reconstruct new dynamic image features, two needle biopsy simulations were used in which the needle motion was either parallel or perpendicular to the frequency encoding direction.

3 Results

Figure 1 shows the results of a simulated contrast-enhanced dynamic imaging study in which (a)-(b) are the reference and dynamic images, respectively, reconstructed using

128 phase encodings. The dynamic changes include a variable rate of enhancement in each of the four lesions as well as a slow overall enhancement in the background tissue. Figure 1 (c)-(e) show the dynamic image reconstructed with SVD, SVD-Keyhole and RIGR, respectively, using 16 dynamic encodings. The images were compared based on the reproduction of the average signal magnitude in the lesions. In addition to having fewer artifacts, the RIGR image faithfully reproduces the signal magnitudes in the lesions whereas the SVD methods do not. This observation is quantified in Fig. 2 which depicts the average signal magnitude in the four lesions. Note that the SVD and SVD-Keyhole images have similar signal magnitudes for all four lesions whereas the RIGR image signal magnitudes are very close to the actual values in the dynamic image (b).

The methods were also tested on real MRI data from a contrast-enhanced dynamic imaging study of a rat with a large breast tumor. A spin echo sequence (TR300/TE20) was used to obtain a high-resolution pre-contrast reference image. The contrast agent was then injected, and a series of dynamic images was acquired. The dynamic data for the RIGR and SVD methods were generated from the measured data as discussed previously. The images were compared based on the reproduction of the spatial features in the lesion. Figure 3(a)-(b) show the reference image and a dynamic image from the series, respectively, reconstructed using 256 phase encodings. Figure 3(c)-(e) show the dynamic image reconstructed using 32 phase encodings with SVD, SVD-Keyhole and RIGR, respectively. In the RIGR image, note the improved delineation of the internal details of the tumor such as those indicated by the arrows.

We next investigate the performance of the methods in capturing new features using a needle biopsy simulation in which the needle motion is either parallel or perpendicular to the frequency encoding direction. The images were compared based on the spatial localization of the needle and the appearance of the artifacts. The first case is shown in Fig. 4, and the second is shown in Fig. 5. In both of these figures, (a)-(b) are the reference and dynamic images, respectively, reconstructed using 256 phase encodings, and (c)-(e) show the dynamic image reconstructed with 32 dynamic encodings using SVD, SVD-Keyhole and RIGR, respectively.

In the parallel case, the SVD methods result in a wide needle reconstruction that appears shifted from the correct location as shown in Fig. 4(c)-(d). In the perpendicular case of Fig. 5(c)-(d), the artifacts manifest as ringing along the axis of the needle which extends across the object in the SVD and SVD-Keyhole images. These artifacts are due to the projection of the ideal image onto the space spanned by the selected reference left singular vectors which contains no information about the needle.

The RIGR images are shown in Fig. 4(e) and Fig. 5(e). Since there is no effective boundary information for the needle present in the reference image, Gibbs ringing resulting from this new feature is evident in the images. However, these artifacts are much less serious than those arising with the SVD methods.

4 Discussion

As discussed in section 2 of this paper, RIGR assumes that a high-resolution reference data set and a reduced set of N dynamic encodings are available. RIGR is an optimal way to mix the two data sets in the reconstruction step (in the cross-entropy sense). The SVD methods also assume that a high-resolution reference image is available. The question the SVD methods attempt to address is, given N excitations, what is the optimal way to encode the dynamic image? If optimal truncated encoding could be accomplished, then neither RIGR nor any other method could do better. The reason that the current SVD methods do not in general produce better images than RIGR is due to the fact that the SVD encodings are optimal only with respect to the reference image and are sub-optimal with respect to the dynamic image (7). In fact, because singular vectors can be very sensitive to perturbation of a matrix (image) (8), the singular vectors derived from the reference image are not just sub-optimal, but they bias the acquisition towards reproducing the dominant features of the reference image.

To demonstrate this point, we calculated the dynamic image using the 32 optimal SVD encodings derived from the high-resolution dynamic image itself. The result is shown in Fig. 6, which is clearly much better than the image in Fig. 4(c) obtained with

32 sub-optimal reference SVD encodings. The non-optimality of the SVD encodings can be significant for applications in which dynamic signal changes are not small.

This problem cannot be remedied by using a Keyhole approach. In fact, with SVD-Keyhole, additional image artifacts can be introduced due to data inconsistency between the reference and dynamic data sets. If the dynamic signal is stronger than the reference signal, the artifacts look similar to an SVD truncation artifact. If the reverse is true, the artifacts look like a high-pass filtered (in the SVD domain) version of the reference image added to the image reconstructed with the low-resolution dynamic data. The latter case is illustrated in Fig. 7 in which (a)-(b) show the reference and dynamic images, respectively, reconstructed using 128 phase encodings. Figure 7 (c)-(d) show the dynamic image reconstructed using 8 dynamic encodings with SVD-Keyhole and RIGR, respectively. Note the edge artifacts that appear in the SVD-Keyhole image of Fig. 7 (c).

An important point worth noting is that, in the simulations used in this study, it was assumed that the selected encoding profiles for the SVD methods could be exactly excited. However, this selective excitation is difficult to achieve in practice, and imperfect excitation will degrade the resulting image (5). In addition, T_1 weighting will further distort the encoded SVD profile when a short T_R is used if T_1 is not uniform across the image. This is especially a problem when a T_1 contrast agent is injected. This is not a problem with RIGR since it uses standard phase encoding.

The RF encoding also limits the application of the SVD methods to single slice or 3D spin echo imaging due to the RF encoding along the one imaging direction. It is also not easy to implement a 2D or thin slab 3D gradient echo sequence for the same reason (9). On the other hand, RIGR can be used with any type of sequence.

5 Conclusion

This paper presents a comparative study of the performance of the RIGR and SVD methods for dynamic imaging applications. Both methods are characterized by the use

of a high-resolution reference image to improve imaging speed. However, RIGR uses the reference information for optimal image reconstruction whereas the SVD methods seek to "optimize" the data acquisition step. Results from this study reveal that, although the SVD encodings are indeed optimal with respect to the reference image, the SVD data acquisition scheme has a tendency to bias the results towards reproducing the known features in the reference image. As a result, the SVD methods have a reduced capability to capture new dynamic image features and contrast changes in existing image features. These characteristics make the SVD methods less suitable for dynamic imaging applications than RIGR.

6 Acknowledgments

The authors thank the anonymous reviewers for helpful suggestions. This work was supported in part by Army Grant #DAMD17-94-J-4126 (JMH)**, NIH Grants PHS-5-P41-RR05964, NSF-RIA Award, the National Center for Supercomputing Applications, the Beckman Institute, the Servants United Foundation, and the Whitaker Foundation.

** The content of this paper does not necessarily reflect the position or the policy of the government, and no official endorsement should be inferred.

References

[1] Z.-P. Liang, P. C. Lauterbur, An efficient method for dynamic magnetic resonance imaging. *IEEE Trans. Med. Imaging* **13**, 677–686 (1994).

[2] J. E. Bishop, I. Soutar, W. Kucharczyk, D. B. Plewes, Rapid sequential imaging with shared-echo fast spin-echo MR imaging, in "Works-in-Progress Proc. Soc. Magn. Reson. Imag. 10th Ann. Meeting, New York, NY, 1992", p. S22.

[3] J. J. van Vaals, H. H. Tuithof, W. T. Dixon, Increased time resolution in dynamic imaging, in "Proc. Soc. Magn. Reson. Imag. 10th Ann. Meeting, New York, NY, 1992", p. 44.

[4] G. P. Zientara, L. P. Panych, F. A. Jolesz, Dynamically adaptive MRI with encoding by singular value decomposition. *Magn. Reson. Med.* **32**, 268–274 (1994).

[5] G. P. Zientara, L. P. Panych, F. A. Jolesz, Keyhole SVD encoded MRI, in "Proc. Soc. Magn. Reson. 2nd Ann. Meeting, San Francisco, CA, 1994", p. 778.

[6] J. M. Hanson, Z.-P. Liang, E. Wiener, P. C. Lauterbur, Fast dynamic imaging using two reference images. *Magn. Reson. Med.* **36**, 172–175 (1996).

[7] Y. Cao, D. N. Levin, On the relationship between feature-recognizing MRI and MRI encoded by singular value decomposition. *Magn. Reson. Med.* **33**, 140–142 (1995).

[8] G. H. Golub, C. F. Van Loan, "Matrix Computations", 2nd ed., John Hopkins University Press, Baltimore, MD, 1989.

[9] L. P. Panych, C. Oesterle, G. P. Zientara, J. Hennig, Implementation of a fast gradient-echo SVD encoding technique for dynamic imaging. *Magn. Reson. Med.* **35**, 554–562 (1995).

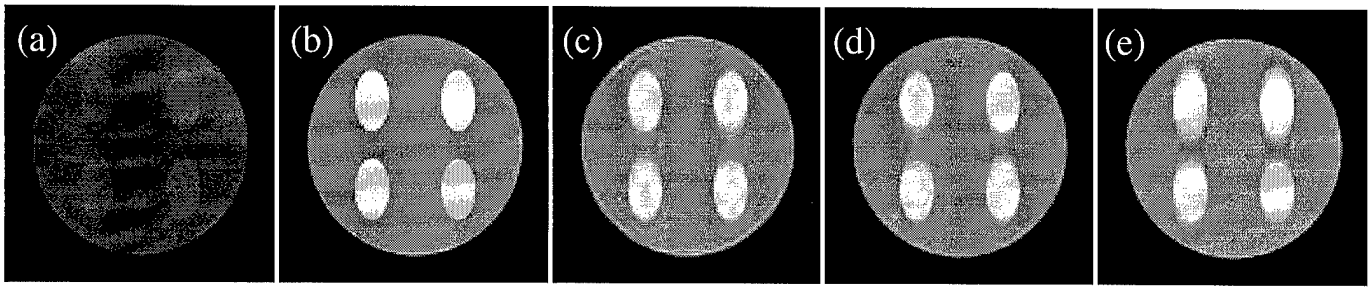

FIG. 1. Contrast-enhanced imaging simulation with all lesions visible in the reference image: (a)-(b) Reference and dynamic images, respectively, reconstructed using 128 phase encodings. (c)-(e) Dynamic image reconstructed with 16 dynamic encodings using SVD, SVD-Keyhole and RIGR, respectively. The SVD encoding direction for the SVD methods and the phase encoding direction for the RIGR method are vertical. Note the improved delineation of the lesions with the RIGR method.

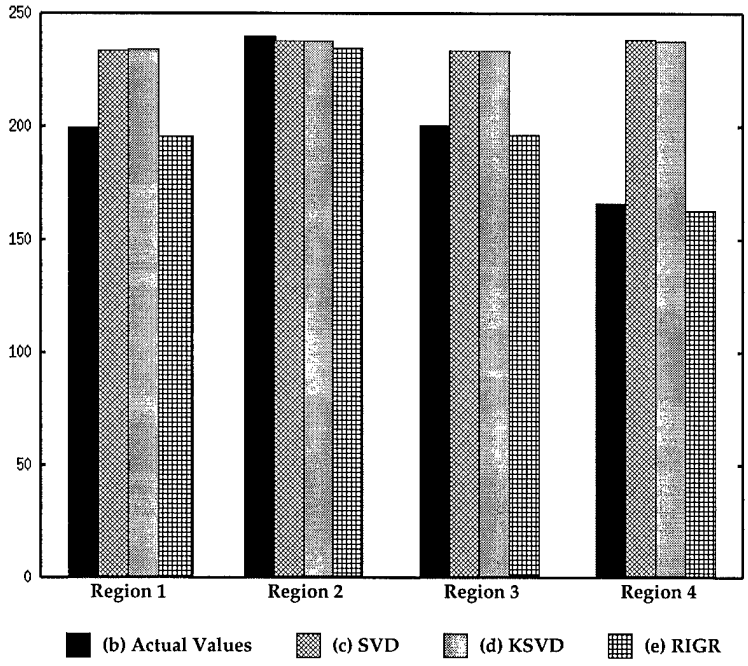

FIG. 2. Average signal magnitude of the lesions in Fig. 1(b)-(e). Note that the SVD methods assign nearly the same average signal magnitude to all four lesions whereas the average signal magnitudes in the RIGR image are quite close to the actual values of the dynamic image (b). (Regions 1, 2, 3 and 4 correspond to the upper left, upper right, lower left and lower right lesions, respectively, in Fig. 1.)

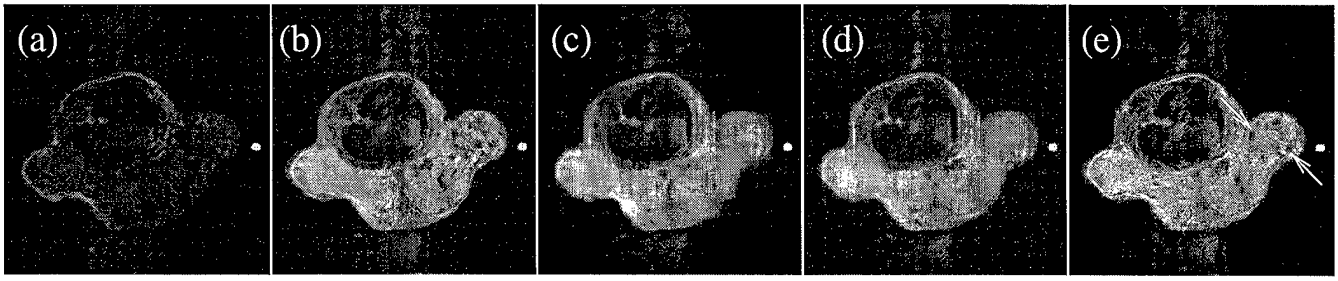

FIG. 3. Contrast-enhanced imaging simulation with rat data: (a)-(b) Reference and dynamic images, respectively, reconstructed using 256 phase encodings. (c)-(e) Dynamic image reconstructed with 32 dynamic encodings using SVD, SVD-Keyhole and RIGR, respectively. The SVD encoding direction for the SVD methods and the phase encoding direction for the RIGR method are vertical. In the RIGR image, note the improved delineation of the internal details of the tumor such as those indicated by the arrows.

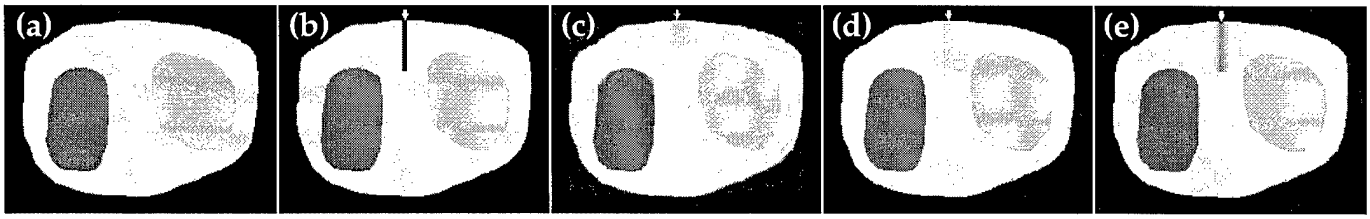

FIG. 4. Needle biopsy simulation with needle motion parallel to frequency encoding direction: (a)-(b) Reference and dynamic images, respectively, reconstructed using 256 phase encodings. (c)-(e) Dynamic image reconstructed with 32 dynamic encodings using SVD, SVD-Keyhole and RIGR, respectively. The SVD encoding direction for the SVD methods and the phase encoding direction for the RIGR method are horizontal. The arrow indicates the center of the needle track. Note the apparent displacement of the needle center in the SVD and SVD-Keyhole reconstructions.

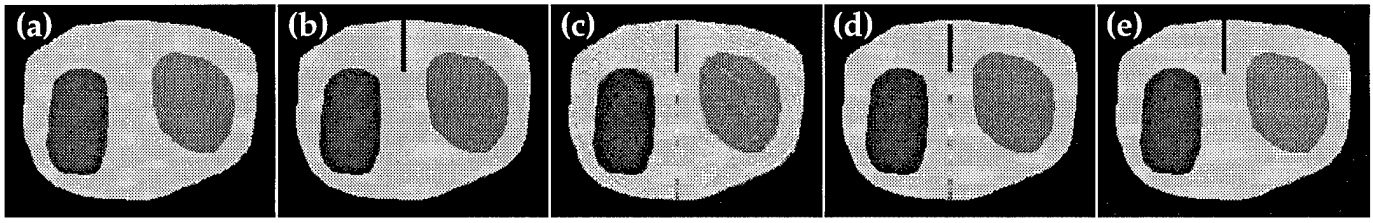

FIG. 5. Needle biopsy simulation with needle motion perpendicular to frequency encoding direction: (a)-(b) Reference and dynamic images, respectively, reconstructed using 256 phase encodings. (c)-(e) Dynamic image reconstructed with 32 dynamic encodings using SVD, SVD-Keyhole and RIGR, respectively. The SVD encoding direction for the SVD methods and the phase encoding direction for the RIGR method are vertical. Note that the ringing artifact which extends across the object in the SVD and SVD-Keyhole images is more localized and less intense with the RIGR method.

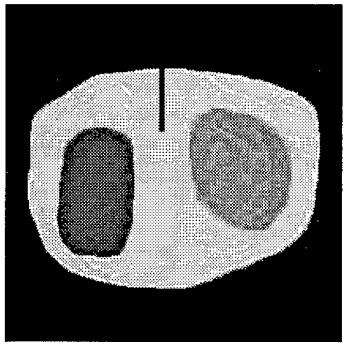

FIG. 6. Optimal dynamic SVD encodings: Dynamic image reconstructed with 32 optimal SVD encodings as derived from the dynamic image itself. The SVD encoding direction is horizontal. Note the improvement over the image in Fig. 4(c) which was reconstructed using the 32 sub-optimal SVD encodings derived from the reference image in Fig. 4(a).

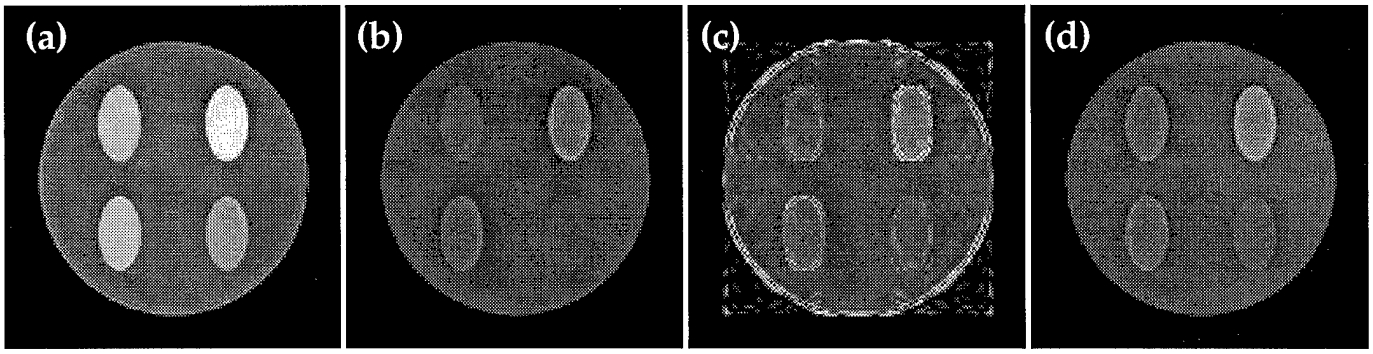

FIG. 7. Illustration of the data inconsistency problem with SVD-Keyhole: (a)-(b) Reference and dynamic images, respectively, reconstructed using 256 phase encodings. (c)-(d) Dynamic image reconstructed with 8 phase encodings using SVD-Keyhole and RIGR, respectively. The SVD encoding direction for the SVD methods and the phase encoding direction for the RIGR method are horizontal. Note the data inconsistency artifacts in the SVD-Keyhole image which are equivalent to a high-pass filtered (in the SVD domain) version of the reference image.

10 Appendix D - Acronyms

BMRL - Biomedical Magnetic Resonance Laboratory

LPA - Localized Polynomial Approximation

MR - Magnetic Resonance

MRI - Magnetic Resonance Imaging

RIGR - Reduced-encoding Imaging by Generalized-series Reconstruction

RSNA - Radiological Society of North America

SMR - Society of Magnetic Resonance

SMRI - Society of Magnetic Resonance Imaging

SMRM - Society of Magnetic Resonance in Medicine

SVD - Singular Value Decomposition

TRIGR - Two reference Reduced-encoding Imaging by Generalized-series Reconstruction

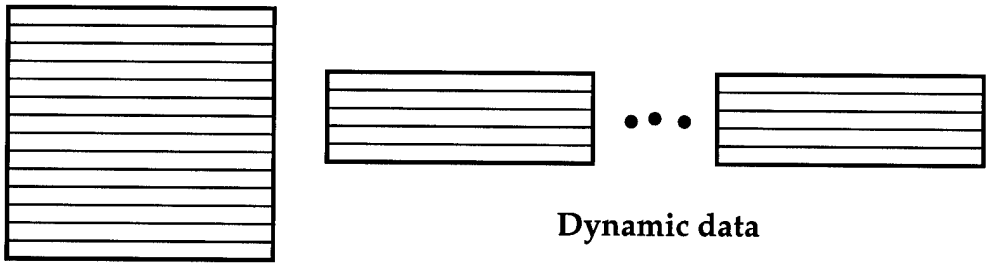

Figure 1: Reduced scan data acquisition scheme: a single high-resolution reference data set is acquired followed by a series of reduced dynamic encodings.

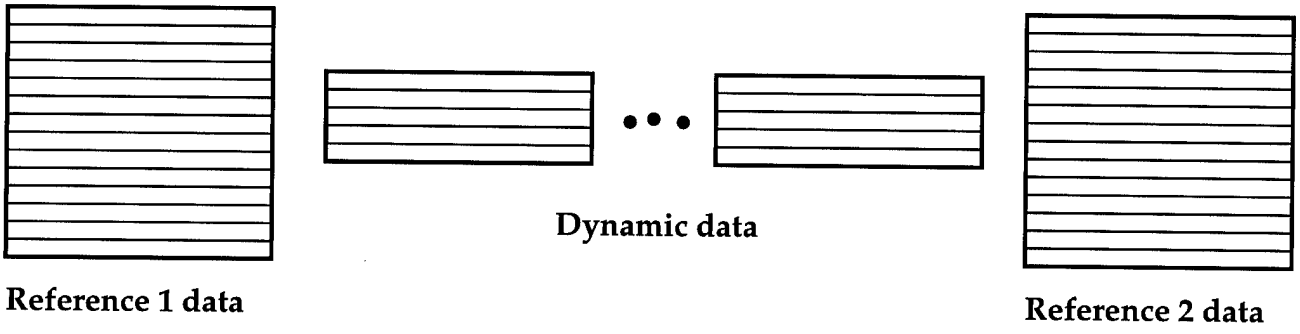

Figure 2: TRIGR data acquisition scheme: two high-resolution reference images, one each for the baseline and active states, and a series of reduced dynamic encodings.

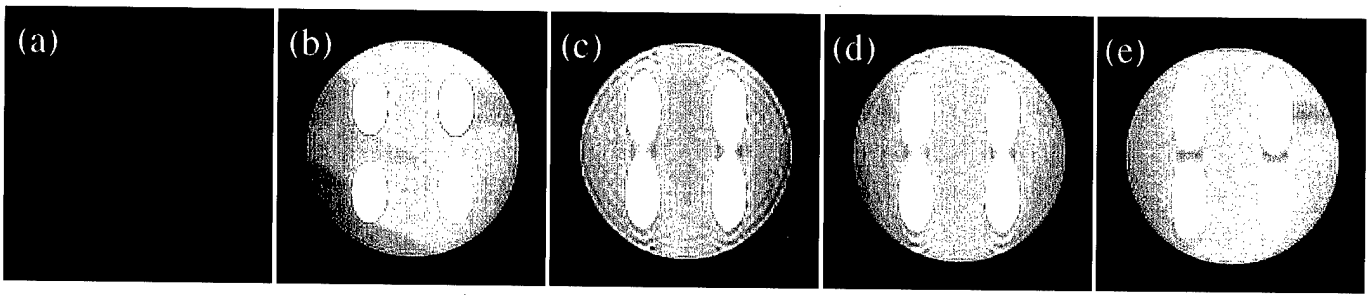

Figure 3: Contrast-enhanced imaging simulation with all lesions visible in the reference image: (a)-(b) Reference and dynamic images, respectively, reconstructed using 128 phase encodings. (c)-(e) Dynamic image reconstructed with 16 dynamic encodings using SVD, SVD-Keyhole and RIGR, respectively. Note the improved delineation of the lesions with the RIGR method.

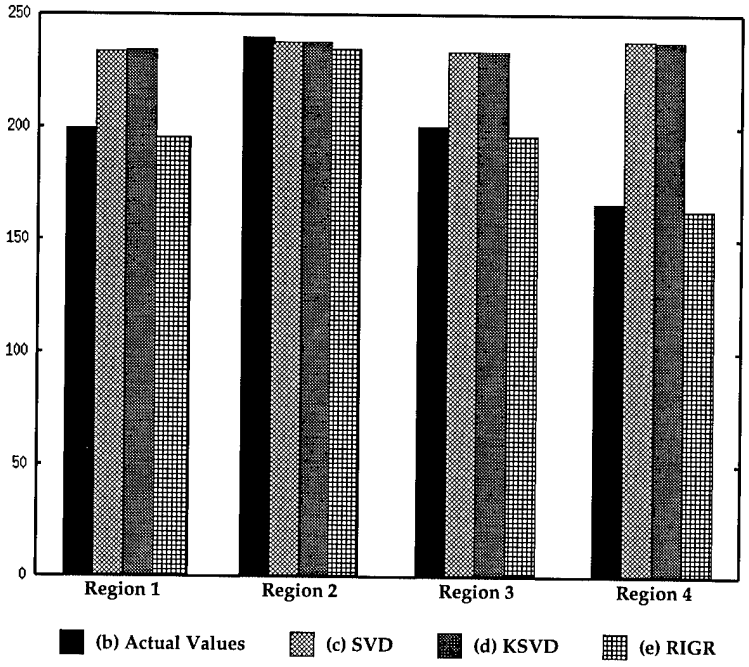

Figure 4: Average signal magnitude of the lesions in Fig. 3(b)-(e). Note that the SVD methods assign nearly the same average signal magnitude to all four lesions whereas the average signal magnitudes in the RIGR image are quite close to the actual values of the dynamic image (b). (Regions 1, 2, 3 and 4 correspond to the upper left, upper right, lower left and lower right lesions, respectively, in Fig. 3.)

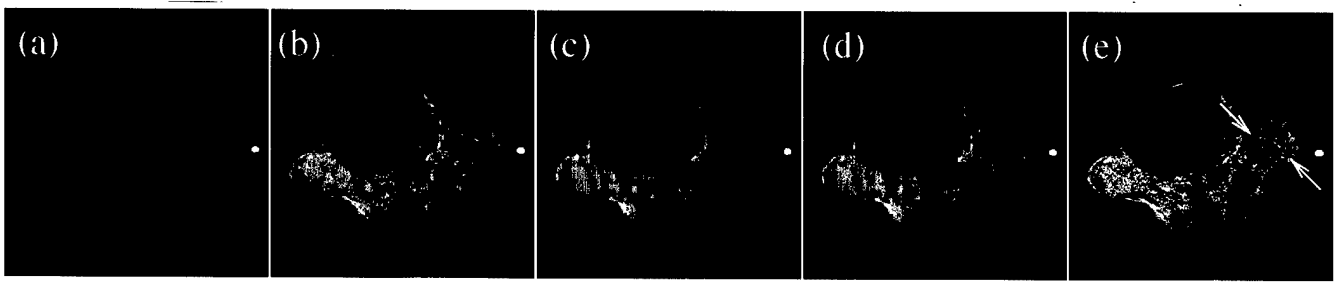

Figure 5: Contrast-enhanced imaging simulation with rat data: (a)-(b) Reference and dynamic images, respectively, reconstructed using 256 phase encodings. (c)-(e) Dynamic image reconstructed with 32 dynamic encodings using SVD, SVD-Keyhole and RIGR, respectively. In the RIGR image, note the improved delineation of the internal details of the tumor such as those indicated by the arrows.

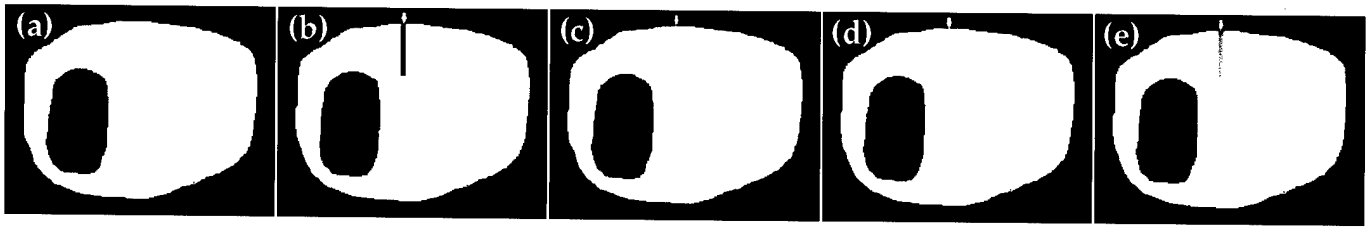

Figure 6: Needle biopsy simulation with needle motion parallel to frequency encoding direction: (a)-(b) Reference and dynamic images, respectively, reconstructed using 256 phase encodings. (c)-(e) Dynamic image reconstructed with 32 dynamic encodings using SVD, SVD-Keyhole and RIGR, respectively. The arrow indicates the center of the needle track. Note the apparent displacement of the needle center in the SVD and SVD-Keyhole reconstructions.

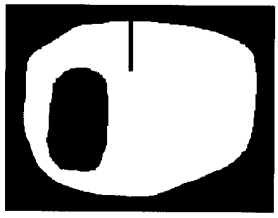

Figure 7: Optimal dynamic SVD encodings: Dynamic image reconstructed with 32 optimal SVD encodings as derived from the dynamic image itself. Note the improvement over the image in Fig. 6(c) which was reconstructed using the 32 sub-optimal SVD encodings derived from the reference image in Fig. 6(a).

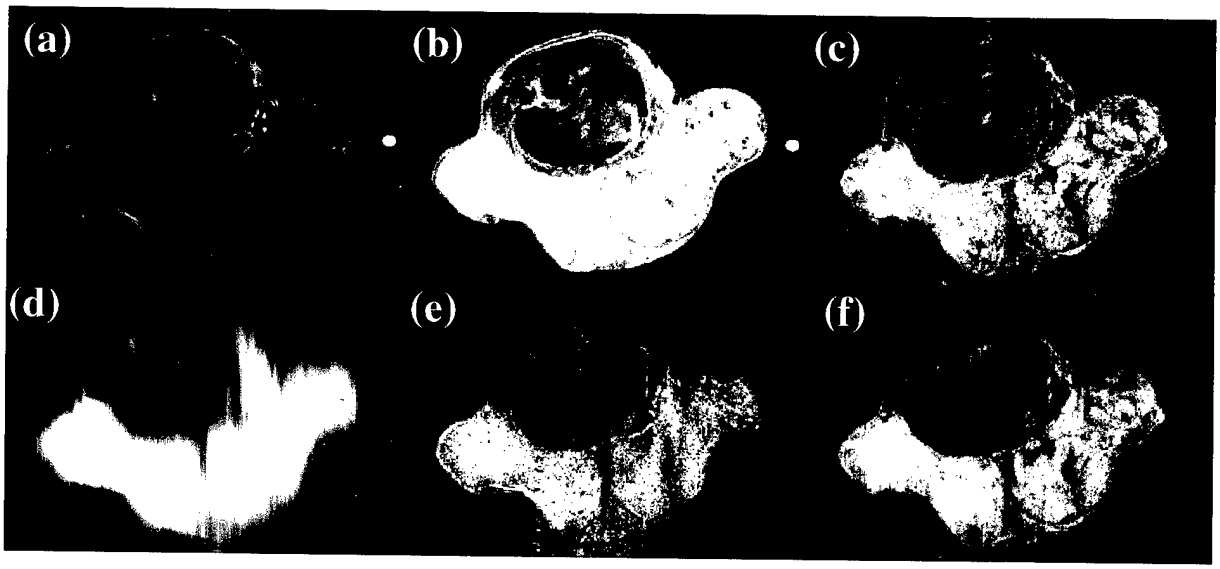

Figure 8: TRIGR results on data from a rat with breast cancer: (a)-(c) pre-contrast reference, post-contrast reference and dynamic change image (difference between a dynamic image (not shown) and the pre-contrast reference image), respectively, reconstructed with 256 phase encodings. (d)-(f) dynamic change image reproduced using only 8 dynamic phase encodings with Keyhole, original RIGR and two-reference RIGR, respectively.

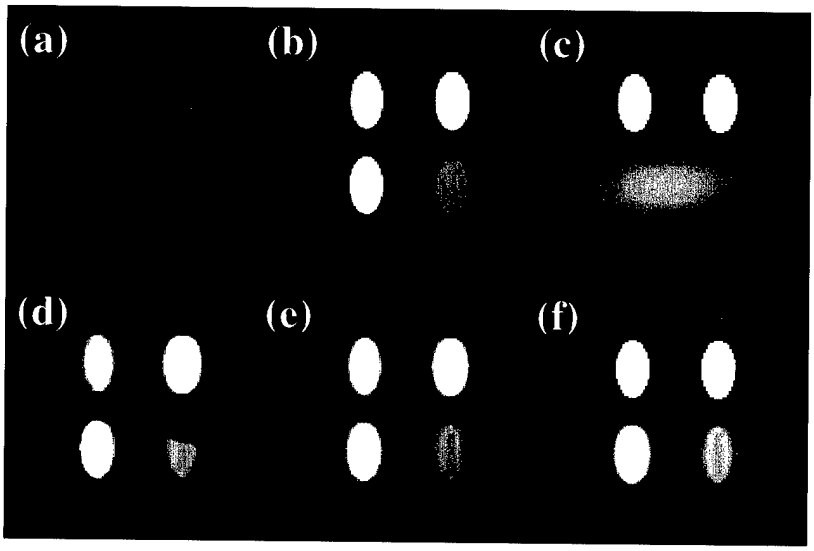

Figure 9: RIGR with Explicit Edge Constraints: (a) and (b) are the reference and dynamic images, respectively, reconstructed using 128 phase encodings. (c) is the new reference created using the fitted dynamic change image and the reference image. (d)-(f) show the dynamic image reconstructed with 32 dynamic encodings using the truncated Fourier method, original RIGR and RIGR with edge constraints, respectively.

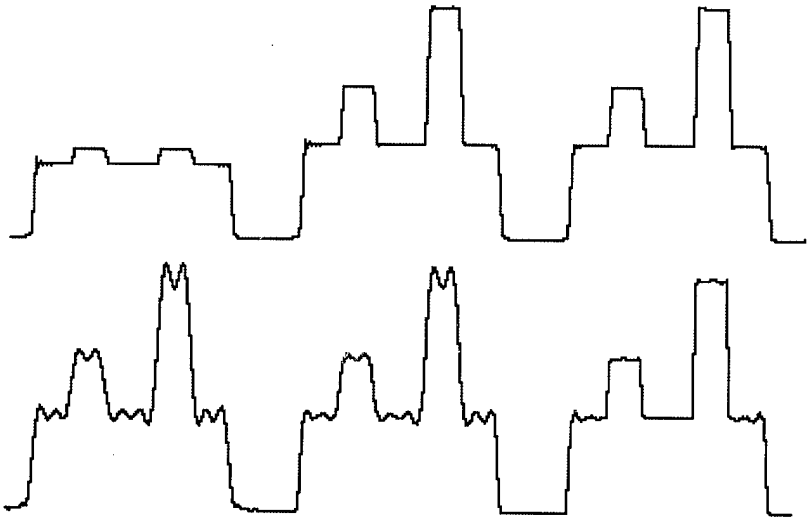

Figure 10: Profiles through the upper set of lesions in Fig. 9.

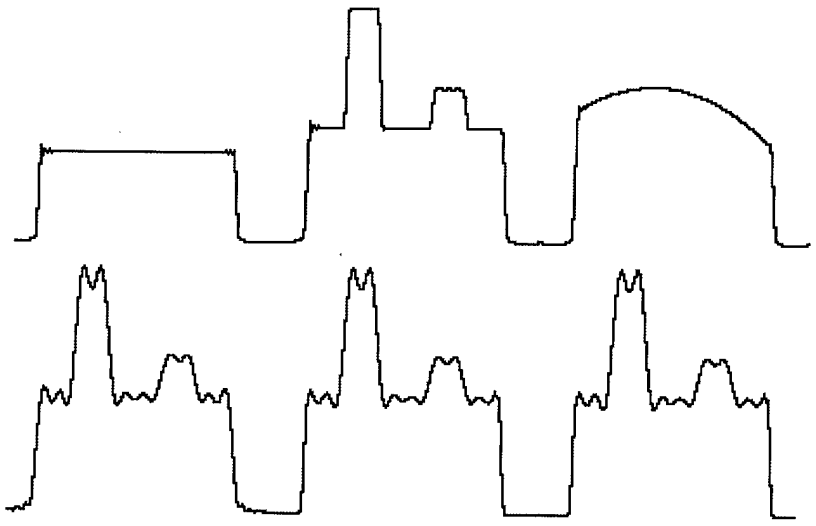

Figure 11: Profiles through the lower set of lesions in Fig. 9.

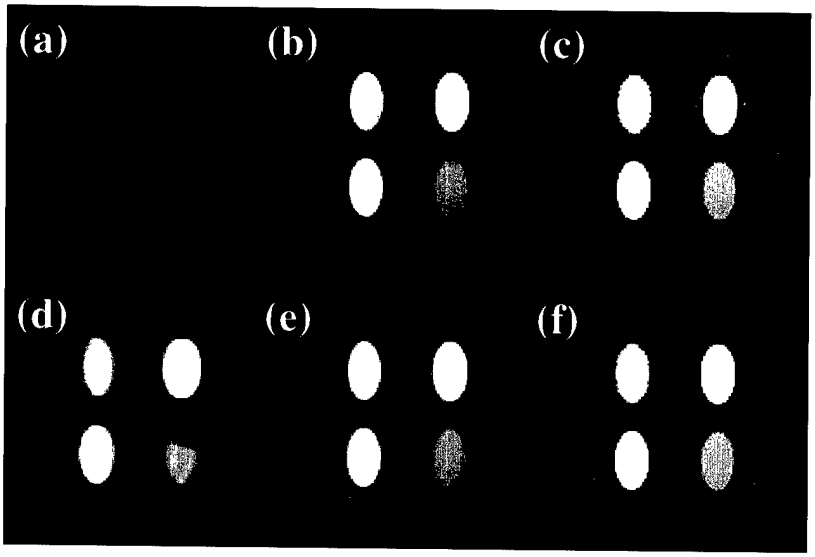

Figure 12: TRIGR with Explicit Edge Constraints: (a) and (b) are the reference and dynamic images, respectively, reconstructed using 128 phase encodings. (c) is the new reference created using the fitted dynamic change image and the reference image. (d)-(f) show the dynamic image reconstructed using 32 dynamic encodings with the truncated Fourier method, original TRIGR and TRIGR with edge constraints, respectively.

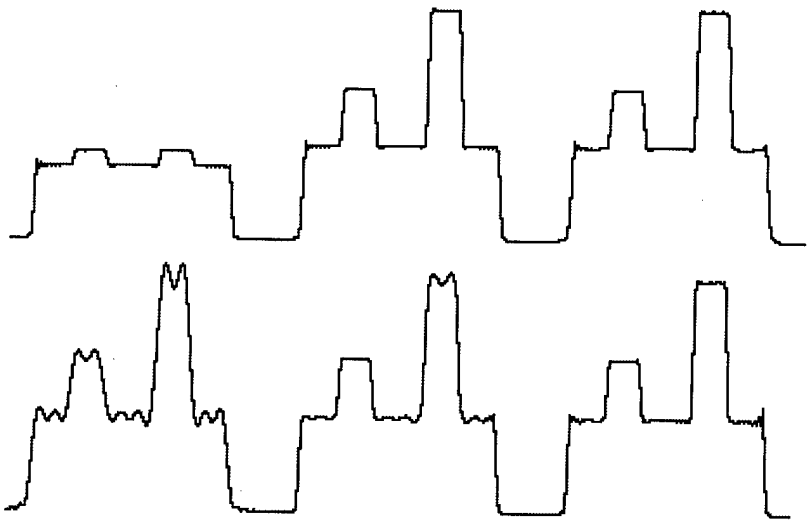

Figure 13: Profiles through the upper set of lesions in Fig. 12.

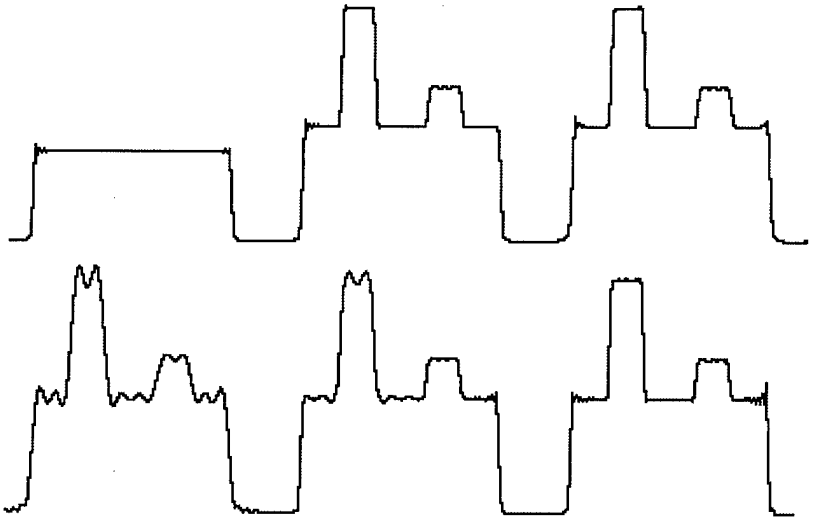

Figure 14: Profiles through the lower set of lesions in Fig. 12.